CONTENTS

A Potential Defense Mechanism Against Amyloid Deposition in Cerebellum

Ph.D Thesis

A dissertation submitted to the Doshisha University in partial fulfillment of the requirements for degree of Doctor of Philosophy

ALAM MD SHAHNUR
ID: 1414172501

Major of Medical Life Systems
Graduate School of Life and Medical Sciences
Doshisha University, Kyoto, Japan

May, 2021

Dedication

I dedicate this thesis to my loving and most respecting

"Father and Mother"

Whose affection, love and encouragement through the entire life make me able to get this success and honour.

List of figures

List of abbreviations

AD, Alzheimer's disease;

Aβ, Amyloid-β;

ISF Aβ, Interstitial fluid Aβ;

APP, Amyloid precursor protein;

CTX, Cerebrum cortex;

CBL, Cerebellum;

CSF, Cerebrospinal fluid;

HF-Aβ42, HiLyte™ Fluor 555 labeled Aβ1-42;

DcLNs, Deep cervical lymph nodes;

HF-Aβ40, HiLyte™ Fluor 555 labeled Aβ1-40;

FAM-scAβ42, 5-Carboxyfluorescein conjugated with scramble Aβ1-42;

Alexa-OV, Alexa Fluor™ 555 conjugated Ovalbumin;

LYVE-1, Lymphatic vessel endothelial hyaluronan receptor-1;

Iba-1, Ionized calcium binding adaptor molecule-1;

Chapter 1

General Introduction

1.1 Alzheimer's disease: Symptoms and Treatment

Alzheimer's disease (AD) is the most common cause of dementia in the elderly people [1]. Clinical characteristics of AD is the progressive loss of cognitive brain function, which lead to degradation of memory, language, behavior and other vital skills, which gradually deteriorates and leads to death [1, 2]. Neuropathological hallmarks of AD are extracellular senile plaque (SP), intracellular neurofibrillary tangle (NFT) and brain atrophy (neuronal loss). SP is composed of amyloid-β (Aβ) peptide and NFT is built up of hyperphosphorylated forms of microtubule associated protein tau [1, 2] (Fig. 1). Symptomatic treatments against AD are available with donepezil, galantamine, rivastigmine, and memantine in the market [3]. Disease-modifying therapeutics is under way so far.

1.2 Aβ as a druggable target against AD

Three autosomal mutations related to onset of AD have been found in amyloid precursor protein (APP), the substrate of Aβ production [4]. These mutations converge on production and aggregation of Aβ. The combination of these findings with neuropathological hallmarks raised the amyloid cascade hypothesis (Fig. 2) [4, 5, 6]. According to this hypothesis, Aβ accumulation triggers tau aggregation which leads to neuronal dysfunction and death (Fig. 2). This concept was further supported by the finding of autosomal dominant mutations in presenilin 1 and 2, components of Aβ producing enzyme γ-secretase, which guided huge numbers of academic and pharmaceutical studies. However, clinical trials based on this

hypothesis has failed so far, which grew calls for the need to reconsider the amyloid hypothesis. In 2012, an APP mutation has been reported to decrease Aβ production and to be related to anti-AD and age-related cognitive decline [7]. Recently the clinical trial on Aducanumab, an anti-Aβ fibril antibody, developed by Biogen and Eisai Ltd., turned out to be promising in late 2019 [8]. They completed submission of biologics license application on this potential antibody drug to the U.S. Food and Drug Administration.

1.3 Production of Aβ

Aβ is derived by proteolysis of type-I transmembrane glycoprotein, APP through cleavage by β-secretase followed by γ-secretase [9, 10]. APP is first cleaved by β-secretase to produce N-terminal soluble fragment (sAPP-β) and C-terminal membrane bound C99 also known as β-carboxyl terminal fragment, βCTF and CTFβ (Fig. 3). γ-Secretase cleaves the transmembrane domain of C99 at 49^{th} or 48^{th} residue to produce APP intracellular domain (AICD) (Fig. 4) [11]. Counter parts of AICD is trimmed down every three residues from their carboxyl terminus to produce Aβ by this enzyme. Importantly, it has been proven that cleavage of C99 at the 49^{th} residue results in Aβ40 production and that cleavage at the 48^{th} leads to aggregation-prone Aβ42 generation by γ-secretase [11]. Aβ42 is the major component of senile plaques in brain and has been considered as a real culprit of AD. This process is known as amyloidogenic pathway. APP can also be processed by α-secretase via non-amyloidogenic pathways to produce non-toxic fragments, which is thought to antagonize Aβ generation [12].

1.4 Progression of Aβ deposition in brain

Senile plaques are generally observed in the basal temporal and orbitofrontal neocortex at early stage of AD brains (Fig. 5 a). Then Aβ deposition is observed throughout the cerebral cortex (CTX), in hippocampal formation, amygdala, diencephalon, and basal ganglia. In severe cases

of AD, senile plaques are also found in mesencephalon, lower brainstem, and cerebellum (CBL) (Fig. 5 a) [13]. Overall, there is a distinct tissue preference in appearance of senile plaques in human brain. An AD model mice tg2576 showed Aβ deposition in a similar fashion to human AD brains (Fig. 5 b) [14]. Robust Aβ deposition in tg2576 brain is observed in CTX. Aβ deposition is barely seen in CBL, although expression level of human APP in brain tissues of tg2576 is 2-3 times higher than endogenous level [15].

1.5 The study aim

As described above, senile plaques and Aβ depositions are dominantly observed in CTX of brains of human and model animals, respectively. Interestingly, NFTs are also mainly found in CTX, but less in CBL. These imply the presence of anti-AD mechanism in CBL. The aim of my study is to figure out the potential mechanism preventing Aβ deposition in CBL. In this study, first I examined the level of Aβ deposition in brain tissues of human APP knock-in mice, $APP^{NL\text{-}G\text{-}F}$, in order to confirm whether these mice can be utilized as AD model animals. Then I further investigated to uncover the mechanism against Aβ deposition in CBL.

Chapter 2

Aβ deposition more in CTX, but less in CBL?

2.1 Brief introduction

Aβ deposition is one of main pathological feature in brains of AD patients and model animals. In addition to Aβ depositions, NFTs are also mainly found in CTX, but less in CBL. These imply the presence of anti-AD mechanism in CBL. The aim of my study is to figure out the potential mechanism preventing Aβ deposition in CBL. To this end, I evaluated levels of Aβ deposition in brain tissues of $APP^{NL\text{-}G\text{-}F}$ mice, in order to confirm whether these mice can be utilized as AD model animals.

2.2 Materials and Methods

2.2.1 Animals

C57BL6 mice; human APP transgenic mice (tg2576); human APP knock-in mice with Swedish, Iberian, and Arctic mutation ($APP^{NL\text{-}G\text{-}F}$). All animal experiments were approved by the animal care and use committee in Doshisha University.

2.2.2 Antibodies

The following primary antibodies used for immunohistochemistry of mouse tissues: 82E1 (1/100 dilution, mouse IgG, IBL) and 6E10 (1/500 dilution, Biolegend) for total Aβ and anti-Iba-1 (1/1,000 dilution, Wako). For 3,3 diaminobenzidine (DAB) staining, 82E1 and 6E10 were used as primary antibodies. Biotinylated anti-mouse rabbit IgG was used as a secondary

antibody (Vector). For fluorescence immunohistochemistry, primary antibodies were detected with the appropriate secondary antibody conjugates with Alexa fluor 488 or 555 (1/500 dilution, Life Technology). 4G8 (1/600 dilution, Biolegend) for immunoprecipitation of Aβ.

2.2.3 Immunohistochemistry

To see the Aβ deposition in APP knock-in and tg2576 mice brain, paraffin-embedded brain sections (6 μm) deparaffinized with xylene and rehydrated in graded ethanol, respectively. After washed twice with PBS, the sections were blocked with 10% goat serum for 1 hour and then incubated with primary each antibody overnight at room temperature. The sections washed with PBS-T and visualized with appropriate secondary antibodies. To analyze the microglial activation, coronal sections were washed twice with PBS-T for 5 minutes and fixed in methanol for 1 hour. Fixed sections were washed twice in PBS-T for 15 minutes and blocked with 10% goat serum for 1 hour. The sections incubated with primary antibody anti-Iba-1. To analyze the glial activation in each specimen to the injection site. 6.4 mm^2 area were analyzed near the injection site to observe phagocytosis of HF-Aβ42 within the activated microglia.

2.2.4 Aβ extraction in brain tissues

Brain tissues were homogenized in four volumes of Tris-buffered saline (TBS) with complete protease inhibitor cocktail using glass-teflon homogenizer on ice. After Ultracentrifugation of the brain homogenate at 100,000 g for 1 hour at 4°C, the supernatant was collected as TS soluble fraction. The pellet was resuspended in four volumes of 50 mM Tris buffer (pH 7.6) containing 6 M Guanidine-HCl by sonication on ice. After incubation for 30 min at room temperature, the resuspension was subjected to ultracentrifugation at 100,000 g for 1 hour at 4°C. This supernatant was collected as TS insoluble fraction. For Aβ isolation, both TS soluble

and insoluble fractions were diluted by addition of 12 volumes of TBS containing 0.1% Tween20 (TBS-T) and subjected to immunoprecipitation with 4G8.

2.2.5 Western blotting

Samples were separated on a 12% gel or 10% gel containing 8 M urea as described previously. [16]. After transferred proteins onto nitrocellulose membrane, the membrane was soaked in boiling phosphate buffered saline for 5 min and incubated in TBSt containing 3% skim milk for 30 min. The membrane was incubated with 82E1 and 6E10 for Aβ and APP detection, respectively. Protein bands were visualized by treating with secondary antibody conjugated with HRP and detected with LAS-4000 (Fujifilm).

2.2.6 *In Vivo* microdiyalysis

The microdialysis experiment was performed as described in [17]. Briefly, the animals were anesthetized with the combination of three anesthetic (50 mg/kg, i.p., Dainippon Sumitomo Pharma), while a guide cannula (4 mm length) was stereotactically implanted in CTX (AP=1.9 mm, ML= 0.5 mm lateral to the midline, and DV= 0.8 mm ventral to surface of skull) and CBL (AP= -1.4 mm, ML=1.5 mm lateral to the midline, and DV=0.8 mm ventral to surface of skull). The guide was fixed using an anchoring bone screw and binary dental cement. At least two days after guide cannula implantation, the mice were placed in a standard microdialysis cage and a probe (Eicom) was inserted through the guide. After insertion of the probe, in order to obtain stable baseline recordings, the probe and connecting tubes were perfused with 0.15% BSA–Ringer's solution for 2 hours at a flow rate of 10 µl/min before baseline sample collection. Samples were collected at a flow rate (0.5 µl/min). Samples were stored at 4 °C in polypropylene tube. Concentrations of human Aβ42 in the dialysate were determined using human Amyloidβ (1-x) Assay kit (IBL). During microdialysis sample collection, mice were

awake and free-moving in the microdialysis cage designed to allow unrestricted movement of the animals without applying pressure on the probe assembly (Eicom).

2.2.7 Stereotaxic injections in brain parenchyma

Mice were anaesthetized with the combination of three anesthetic (50 mg/kg, i.p., Dainippon Sumitomo Pharma) in PBS and the head was secured in a stereotaxic frame. An incision was made in the skin to expose the skull and a hole was drilled at +1 mm in AP, -1.5 mm in ML, and 1.8 mm in the DV for cortex injection. For cerebellum, injection was performed at -7.0 mm in AP, -1.5 mm in ML, and 2.0 mm in the DV. HiLyte™ Fluor 555 labeled Aβ42 (HF-Aβ42, Thermofisher) was dissolved in artificial cerebrospinal fluid (CSF, Tocris Bioscience) at a concentration of 2 mg/ml and injected into brain tissues as described above. After injection, the syringe left in place for additional 2 min to prevent backflow.

2.2.8 Statistical analysis

Paired and un-paired *t*-test were used to compare the difference of groups. All data are shown as means ± SD, and statistical significance was assessed at $p < 0.05$.

2.3 Results

2.3.1 Distribution of Aβ deposition in *APP*$^{NL\text{-}G\text{-}F}$ mice brain

There is an obvious tendency that Aβ deposition is mainly observed in CTX in AD brains and human APP overexpressing mouse model, tg2576 (Fig. 5) [13, 14]. Aβ deposition in CBL is so less that amyloid accumulation visualized with Pittsburgh compound-B in CTX is shown in reference to that in CBL in AD imaging diagnosis [18]. The CBL in tg2576 also exhibits less

Aβ deposition compared to their CTX, although APP is overexpressed under the control of prion promoter. Recently, human APP knock-in mice (*APP*$^{NL-G-F}$) were established as the next generation AD model mice in which aggregation prone Aβ42 is produced predominantly in whole brain [19]. However, it is unknown whether these mice show similar distribution of Aβ deposition as observed in AD brains, although they express human APP under the control of mouse endogenous promoter. It is very important to confirm whether these mice show the same pathological features to AD brains. To this end, I performed immunohistochemical analysis of *APP*$^{NL-G-F}$ mice. I detected more Aβ deposition in CTX, but less in CBL (Fig. 6) [20], suggesting that *APP*$^{NL-G-F}$ can be utilized for further my study as AD model mice.

2.3.2 Total Aβ level in CTX and CBL

Although CBL exhibited less Aβ deposition than CTX on *APP*$^{NL-G-F}$, one may assume that Aβ in CBL remain undetectable by immunohistochemical technique largely due to forming diffuse oligomers rather than distinct aggregates and that the total amount of Aβ in CBL is equivalent to that in CTX. To test this possibility, I extracted Aβ from brain tissues of *APP*$^{NL-G-F}$ mice in 6 M guanidine hydrochloride and performed immunoprecipitation followed by Western blotting for Aβ detection. I detected no significant difference in Aβ level between CTX and CBL in 1- and 3-week mice (Fig. 7). However, levels of Aβ from CTX after 7 weeks significantly elevated, compared to those from CBL, regardless of comparable APP expression [20]. I also quantitated soluble and insoluble Aβ from CTX and CBL in 3-, 7- and 13-week *APP*$^{NL-G-F}$ mice (Fig. 8). I observed less difference of soluble Aβ level between CTX and CBL but this difference was increased in insoluble Aβ. These data suggest that age-dependent elevation of Aβ level reflects Aβ deposition in brain tissues, especially in CTX.

2.3.3 Interstitial fluid Aβ levels in CTX and CBL

I observed significant elevation of Aβ level especially in CTX by aging. However, it is unclear whether the Aβ elevation is due to increase in Aβ production or Aβ accumulation. To examine Aβ production levels in brain issues, my collaborator, Dr. M. Nakano measured interstitial fluid (ISF) Aβ in CTX and CBL by using microdialysis. Because ISF Aβ can be considered as Aβ right after production or prior to deposition in brain. As shown in Fig. 9, the amount of ISF Aβ in CTX was equivalent to that in CBL [20]. This data suggests that less Aβ deposition in CBL is related to enhanced Aβ clearance, rather than Aβ production level.

2.3.4 Microglial activation in CTX and CBL

It is reported that microglia cells play a role on Aβ clearance [21]. One may assume that microglia cells are activated to remove Aβ via phagocytosis in CBL, resulting in less Aβ deposition in CBL. To test this possibility, I investigated the microglial activation in CTX and CBL on injection of HiLyte™ Fluor 555 labeled Aβ1-42 (HF-Aβ42) into brain tissues. It is interesting to note that HF-Aβ42 formed punctate and filamentous structures in CTX and CBL, respectively (Fig. 10). However, I observed no significant difference in HF-Aβ42 engulfment within Iba-1 positive microglias in brain regions (Fig. 10) [20]. This data suggests that Aβ clearance in CBL is mediated by a mechanism other than microglial phagocytosis.

Taken together, I observed less Aβ level in CBL. But it is not the result of less Aβ production efficiency or enhanced microglial phagocytosis in CBL than that of CTX. These results further influence me to examine the clearance rate of Aβ in CTX and CBL.

Chapter 3

Aβ diffusion in CTX and CBL

3.1 Brief introduction

I found that Aβ deposition was less in CBL compared to CTX, in *APP*$^{NL\text{-}G\text{-}F}$ mice, as observed in brains of AD patients and tg2576 mice. However, no significant difference was detected in the levels of ISF Aβ between CTX and CBL. I also failed to detect significant difference in microglial engulfment of Aβ in those brain tissues. It is still unclear why more Aβ deposition is detected in CTX, but less in CBL. Here I focused on Aβ diffusion as a part of Aβ clearance in brain tissues.

3.2 Materials and Methods

3.2.1 Stereotaxic injections in brain parenchyma

Mice were anaesthetized with the combination of three anesthetic (50 mg/kg, i.p., Dainippon Sumitomo Pharma) in PBS and the head was secured in a stereotaxic frame. An incision was made in the skin to expose the skull and a hole was drilled at +1 mm in AP, -1.5 mm in ML, and 1.8 mm in the DV for cortex injection. For cerebellum, injection was performed at -7.0 mm in AP, -1.5 mm in ML, and 2.0 mm in the DV. Using a Hamilton syringe (26-gauge needle), 0.5 μl of HiLyte™ Fluor 555 labeled Aβ42 (HF-Aβ42; 0.5 mg/ml and 2 mg/ml), 5-carboxyfluorescein conjugated scramble Aβ42 (FAM-scAβ42; 2 mg/ml), and Alexa Fluor™ 555 conjugated Ovalbumin (Alexa-OV; 2 mg/ml) were injected. After injection, the syringe

left in place for additional 2 min to prevent backflow. HF-Aβ42 and FAM-scAβ42 peptides were purchased from Thermofisher and Alexa-OV from Anaspec INC. All the peptides dissolved in artificial cerebrospinal fluid (CSF) (Tocris Bioscience).

3.2.2 Immunohistochemistry

Mice were sacrificed by cervical dislocation under anesthesia and removed brains. Tissues were fixed in 4% paraformaldehyde (PFA) for 48 hours. After stripping the skin and muscle from the bone, the brain fixed in 4% PFA for 48 hours. Fixed tissues were washed and soaked in PBS for 24 hours. To see the Aβ in brain tissues after HiLyte™ Fluor 555 labeled Aβ injection in C57BL6 mice, paraffin-embedded brain sections (6μm) deparaffinized with xylene and rehydrated in graded ethanol, respectively. After washed twice with PBS, the sections were blocked with 10% goat serum for 1 hour and then incubated with primary each antibody overnight at room temperature. The sections washed with PBS-T and visualized with appropriate secondary antibodies

3.2.3 Statistical analysis

Paired and un-paired *t*-test were used to compare the difference of groups. All data are shown as means ± SD, and statistical significance was assessed at $p < 0.05$.

3.3 Results

3.3.1 Injected Aβ42 in CTX and CBL

To gain insight into potential enhanced Aβ clearance in CBL, I applied stereotaxic injection of HiLyte™ Fluor 555 labeled Aβ1-42 (HF-Aβ42) into CTX and CBL and observed its temporal

distribution in the brain tissues (Fig. 11 a). Brain tissues were removed at each time course and brain slices were examined HF-Aβ42 distribution. At low concentration (0.5 mg per ml), diffusion areas of HF-Aβ42 in CBL were roughly six-times larger than those in CTX at 0 h (right after injection) (Fig. 11 a). HF-Aβ42 positive area in CTX tended to be consistent up to 72 h after injection. In contrast, HF-Aβ42 positive area in CBL showed 88% reduction at 24 h after injection (Fig. 11 b and c) [20].

At high concentration (2 mg per ml), diffusion areas of HF-Aβ42 in CBL were roughly four-times larger than those in CTX at 0 h (Fig. 12 a). HF-Aβ42 positive area in CTX tended to constant up to 72 h after injection. In contrast, HF-Aβ42 positive area in CBL showed 75% reduction at 72 h after injection (Fig. 12 b and c). These data suggest that Aβ42 in CBL is more diffusive and cleared out faster than that in CTX.

3.3.2 Immunological detection of Aβ42 from HF-Aβ42 in brains

I detected HF-Aβ42 in brain tissues even in three days after stereotaxic injection. To confirm HF-Aβ42 fluorescence reflects Aβ distribution, I performed immunostaining with anti-Aβ antibody, 4G8 on injected specimens. As shown in Fig. 13, HF-Aβ42 fluorescent patterns merged with 4G8 signals, suggesting that HF-555 localization reflects a bona fide Aβ distribution.

3.3.3 Injected Fam-ScAβ42 in CTX and CBL

In order to examine whether the observation above is dependent of Aβ42 sequence or not, I injected scrambled sequence of Aβ42 conjugated with 5-carboxyfluorescein (FAM-scAβ42). A significant diffusive distribution of FAM-scAβ42 in CBL, compared to that in CTX, right after injection (Fig. 14 a and b). However, FAM-scAβ42 was cleared out from CBL, similar to

that from CTX (Fig. 14 b). I detected no significant difference in normalized FAM-scAβ42 distributions overtime (Fig. 14 c) [20]. This indicates that faster Aβ42 disappearance in CBL depends on Aβ42 sequence.

3.3.4 Injected Aβ40 in CTX and CBL

It has been reported that Aβ42 is more aggregative than Aβ40 [22]. One may assume that less aggregative Aβ40 could cleared from CTX. In order to investigate this issue, I stereotactically injected HiLyte™ Fluor 555 labeled Aβ1-40 (HF-Aβ40) in these brain tissues. Diffusion areas of HF-Aβ40 in CBL were roughly six-times larger than those in CTX at 0 h (right after injection) (Fig. 15). HF-Aβ40 positive area in CTX tended to increase gradually up to 72 h after injection. In contrast, HF-Aβ40 positive area in CBL showed 55% reduction at 72 h after injection (Fig. 15 b and c). This data indicate that Aβ40 in CBL is more diffusive and cleared out faster than that in CTX.

3.3.5 Immunological detection of HF-Aβ40 in brains

I detected HF-Aβ40 in brain tissues even in three days after stereotaxic injection. To confirm HF-Aβ40 fluorescence reflects Aβ distribution, I performed immunostaining with anti-Aβ antibody, 4G8 on injected specimens, as performed on HF-Aβ42 above. As shown in Fig. 16, HF-Aβ40 fluorescent patterns merged with 4G8 signals, suggesting that HF-555 localization reflects a bona fide Aβ distribution.

3.3.6 Injected Alexa-OV in CTX and CBL

As described above, I observed rapid Aβ diffusion and clearance in CBL, in an Aβ sequence dependent manner. To gain insights into diffusion and clearance of higher molecular weight

protein than Aβ, I injected Alexa Fluor™ 555 conjugated Ovalbumin (Alexa-OV) in brain tissues. Diffusion areas of Alexa-OV in CBL were roughly six-times larger than those in CTX at 0 h (right after injection) (Fig. 17). Alexa-OV positive area in CTX and CBL tended to decrease gradually up to 72 h after injection. Alexa-OV positive area in CTX and CBL showed 95% and 99% reduction, respectively after 72 hours of injection (Fig. 17 b and c) [20]. Normalized data suggests that clearance patterns of ovalbumin between CTX and CBL are similar each other, although CBL exhibits fast diffusion of ovalbumin right after injection.

Taken together, my data demonstrate that Aβ is more cleared from CBL due to higher diffusion rate than in CTX. However, it is unknown the destination of this cleared Aβ. These results further influence me to examine the drainage of Aβ from brain to DcLNs.

Chapter 4

Enhanced drainage of Aβ from CBL into deep cervical lymph nodes

4.1 Brief introduction

I have observed diffusion area expand in CBL than CTX after Aβ injection. The Aβ diffusion area is decreased in CBL over the times but not in CTX that indicate Aβ is more cleared from CBL due to higher diffusion rate than in CTX. However, it is unknown the destination of this cleared Aβ. Recently meningeal lymphatic system around the brain has been re-discovered [20]. Cerebrospinal fluid is cleared outside of central nervous system into deep cervical lymph nodes (DcLNs) after drainage from the basal meningeal lymphatic vessels [23]. Here I focused on lymphatic drainage system including DcLNs as a part of Aβ clearance in CBL.

4.2 Materials and Methods

4.2.1 Animals

C57BL6 mice; human APP knock-in mice with Swedish and Iberian mutation (APP^{NL-F}). All animal experiments were approved by the animal care and use committee in Doshisha University.

4.2.2 Antibodies

The following primary antibodies used for immunohistochemistry of mouse tissues: 82E1 (1/100 dilution, mouse IgG, IBL), Monoclonal anti-mouse LYVE-1 (1/200, rat IgG, Invitrogen) and Polyclonal anti-Aβ42 (1/100 dilution, rabbit IgG, IBL). For 3,3 diaminobenzidine (DAB) staining, 82E1 was used as primary antibodies. Biotinylated anti-mouse rabbit IgG was used as a secondary antibody (Vector). For fluorescence immunohistochemistry, primary antibodies were detected with the appropriate secondary antibody conjugates with alexa fluor 488 or 555 (1/500, Life Technology).

4.2.3 Stereotaxic injections in brain parenchyma

Mice were anaesthetized with the combination of three anesthetic (50 mg/kg, i.p., Dainippon Sumitomo Pharma) in PBS and the head was secured in a stereotaxic frame. An incision was made in the skin to expose the skull and a hole was drilled at +1 mm in AP, -1.5 mm in ML, and 1.8 mm in the DV for cortex injection. For cerebellum, injection was performed at -7.0 mm in AP, -1.5 mm in ML, and 2.0 mm in the DV. Using a Hamilton syringe (26-gauge needle), 0.5 µl of HiLyte™ Fluor 555 labeled Aβ42 (HF-Aβ42; 2 mg/ml) and Alexa Fluor™ 555 conjugated Ovalbumin (Alexa-OV; 2 mg/ml) were injected. After injection, the syringe left in place for additional 2 min to prevent backflow.

4.2.4 Immunohistochemistry

Mice were sacrificed by cervical dislocation under anesthesia and removed brains and DcLNs. Tissues were fixed in 4% paraformaldehyde (PFA) for 48 hours. To see the Aβ deposition in APP knock-in *APP*$^{NL-F}$ mice brain, paraffin-embedded brain sections (6µm) deparaffinized with xylene and rehydrated in graded ethanol, respectively. After washed twice with PBS, the sections were blocked with 10% goat serum for 1 hour and then incubated with primary each antibody overnight at room temperature. The sections washed with PBS-T and visualized with

appropriate secondary antibodies. For DcLNs, tissues were cryoprotected with 30% sucrose buffer before making sections. Frozen DcLNs sliced with 30-μm thick sections using a cryostat (Leica CM1950) at −20°C. To see the Aβ in DcLNs tissues after HiLyte™ Fluor 555 labeled Aβ injection in C57BL6 mice brain, the sections were blocked with 10% goat serum for 1 hour and then incubated with primary each antibody overnight at room temperature. The sections washed with PBS-T and visualized with appropriate secondary antibodies**.** Images acquired with confocal microscope (LSM 700; Carl Zeiss Inc.). Quantitative analysis using the acquired images was performed using image J software.

4.2.5 Statistical analysis

Paired and un-paired *t*-test were used to compare the difference of groups. All data are shown as means ± SD, and statistical significance was assessed at $p < 0.05$.

4.3 Results

4.3.1 Rapid drainage of HF-Aβ42 into deep cervical lymph nodes from CBL

Recently meningeal lymphatic system around the brain has been re-discovered [23]. Cerebrospinal fluid is cleared outside of central nervous system into deep cervical lymph nodes (DcLNs) after drainage from the basal meningeal lymphatic vessels [24]. To examine whether Aβ injected into brain tissues was drained into DcLNs, I isolated DcLNs from mice injected with HF-Aβ42 and stained with anti-lymphatic vessel endothelial hyaluronan receptor-1 (LYVE-1) antibody. I detected faint HF-Aβ42 fluorescence in 2 h after injection in CTX (Fig. 18). In contrast, HF-Aβ42 was robustly detected in DcLNs within 2 h and gradually reduced toward 72 h after injection in CBL [20].

4.3.2 Immunological detection of CBL injected HF-Aβ42 in DcLNs

As described above, I robustly detected HF-Aβ42-derived fluorescence in DcLNs after three days of CBL injection. However, it is unclear whether HF-Aβ42 is intact in DcLNs or not. One may assume that HiLyte™ Fluor 555 signal in DcLNs is derived from degradation product of HF-Aβ42. To exclude this possibility, I performed immunostaining of DcLNs with anti-Aβ42 antibody. Fluorescent pattern of anti-Aβ antibody partially merged with HiLyte™ Fluor 555 signal, suggesting that HF-Aβ42 is intact in DcLNs (Fig. 19).

4.3.3 Drainage of Alexa-OV from brain into DcLNs

I also monitored transportation of macromolecules Alexa-OV from brain into DcLNs. I isolated DcLNs from mice injected with Alexa-OV and stained with anti-lymphatic vessel endothelial hyaluronan receptor-1 (LYVE-1) antibody. Alexa-OV appeared in DcLNs from CTX within 2 hours of injection and declined gradually thereafter (Fig. 20 a and b). Nonetheless, Alexa-OV drainage from CBL increased at a delayed time point and peaks at 24 hours. Quantitative data showed that transport of Alexa-OV was significantly higher from CTX at 2 h compared to CBL whereas after 24 h Alexa-OV was significantly higher in CBL compared to CTX (Fig. 20 b). This data indicate that high molecular weight protein drainage pattern is different from Aβ.

4.3.4 Drainage of endogenous Aβ into DcLNs from brain

I detected robust HF-Aβ in DcLNs after CBL injection (Fig. 18). However, one may assume that this is experimental artifact caused by high dose injection. To examine whether Aβ is drained into DcLNs even in physiological condition, I isolated DcLNs from $APP^{NL\text{-}F}$ mice. Interestingly, I detected robust Aβ-specific signals in 14-month old mice (Fig. 21) [20]. It is important to note a tendency of age-dependent increase of Aβ in DcLNs. Although it is

unknown whether Aβ detected in DcLNs is derived from CBL, this data imply that Aβ from CBL is drained into DcLNs rather than the CTX with aging.

Taken together, these results indicate that more Aβ accumulated in DcLNs from CBL is due to the higher drainage activity of CBL.

Chapter 5

Discussion

5.1 Aβ deposition in CTX and CBL

The accumulation of Aβ peptides in the brain parenchyma has been thought to be related to the pathogenesis AD. However, the precise mechanism of pathogenicity is still unclear. Amyloid plaques first accumulate in the CTX, followed by accumulation in the CBL as the disease progresses [25]. In this study, immunohistochemical analyses revealed less Aβ deposition in CBL compared to CTX in human APP knock-in mice, $APP^{NL\text{-}G\text{-}F}$ (Fig. 6) [20]. These imply that CBL may have anti-AD mechanism that ultimately causes less Aβ deposition in CBL than CTX. The potential interpretation why CBL forms less Aβ deposition would be reduced expression of substrate or enzymes on Aβ production in CBL. However, Human Protein Atlas (https://www.proteinatlas.org) indicates that RNA expression levels for Aβ producing genes such as APP, BACE1, Preseniline, and Nicastrin in CTX are only about 2 times higher than those in CBL [26]. It is not reasonable to consider that such a difference on expression levels is enough to explain the difference on Aβ deposition between CTX and CBL. Alternatively, it is possible that the level of Aβ deposition in CBL is under rated due forms Aβ oligomers which is invisible in regular staining technique. If so, the total amount of Aβ in CBL would be equivalent to that in CTX. To test this possibility, I quantitated total Aβ level in CTX and CBL of $APP^{NL\text{-}G\text{-}F}$ mice. Although I found no difference in total amount of Aβ level in young mice, total Aβ level was 4.5 times higher in CTX than CBL (Fig. 7) [20]. These data indicate that the level of Aβ deposition reflects the amount of Aβ in brain tissues.

5.2 Reduced level of Aβ in CBL

It is unknown why CBL contains reduced amount of Aβ compared to CTX, although expression levels of APP and Aβ producing enzymes are comparable between CTX and CBL. One possible interpretation is less Aβ production and other possibility is less Aβ accumulation in CBL, compared CTX. Microdialysis analysis on $APP^{NL\text{-}G\text{-}F}$ mice revealed the level of ISF Aβ in CBL was roughly 80% of that in CTX (Fig. 9) [20]. It is unlikely that 20% reduction in Aβ production in CBL leads to less Aβ deposition. In addition to this, levels of TS soluble Aβ in CTX and CBL at the age of 7 weeks were similar to each other (Fig. 8a). It is reasonable to consider that less Aβ level in CBL is due to less Aβ accumulation, rather than less Aβ production.

5.3 Reduced Aβ accumulation and clearance in CBL

It is likely that Aβ accumulation is dependent on the environment surrounding Aβ monomers and Aβ clearance conditions. Juri Togashi in Neuropathological laboratory performed a set of aggregation assay on Aβ42 in the presence of lysates of CTX and CBL. Although such *in vitro* assays were artificial, she failed to detect significant difference in Aβ42 aggregation between CTX and CBL lysates (Togashi and Funamoto, unpublished). In this study, I focused on Aβ clearance in brain tissues. Aβ degrading enzymes, such as neprilysin, insulin-degrading enzyme, endothelin-converting enzyme, plasminogen activator, angiotensin-converting enzyme, and matrix metalloproteinases may reduce Aβ level in CBL [27] and Neprilysin is thought to be a major Aβ degrading enzyme. However, Human Protein Atlas (https://www.proteinatlas.org) indicates 6-times reduction in neprilysin expression level in CBL, which suggest that Aβ degrading enzymes may not contribute to less Aβ accumulation in CBL [26].

I examined microglial activation after injection HF-Aβ42 and compare microglial engulfment of HF-Aβ42 between CTX and CBL. But I failed to detect a significant difference of HF-Aβ positive microglia cell between CTX and CBL (Fig. 10) [20].

5.4 Aβ diffusion in CBL

Regarding Aβ clearance, I focused on the diffusion rate of Aβ in brain tissues. Injected HF-Aβ42 in the CBL expanded about six-times than CTX at 0 hour and decreased sharply after 24 hours from CBL (Fig. 11) [20]. The CBL showed 88% and 99% reduction of HF-Aβ42 respectively at 24 hours and 72 hours whereas the HF-Aβ42 positive area in CTX was consistent up to 72 hours after injection (Fig. 11) [20]. I examined scramble Aβ42 (FAM-scAβ42) diffusion in brain. Interestingly, I observed a similar reduction of FAM-scAβ42 in CTX and CBL after 72 hours (Fig. 14) [20]. This finding indicates that less reduction of Aβ42 from CTX is depends on Aβ42 sequence. Then, I examined a relatively higher molecular weight protein, Ovalbumin (Alexa-OV). The Alexa-OV decreased over times and reduction rate is similar between CTX and CBL (Fig. 17) [20]. These data suggest that less Aβ accumulation in CBL is due to diffusion mediated faster clearance from CBL and less clearances in CTX depends only Aβ sequence but not molecular size of a molecule.

5.5 Aβ drainage into DcLNs

It has been reported that brain CSF moves into DcLNs through basal meningeal lymphatic vessels, although precise mechanistic pathway still unknown [24]. The drainage of fluorescent tracers from the brain parenchyma has been extensively studied [28-32]. In particular, Balint and his colleague reported the drainage of 70 kDa and 40 kDa Rhodamine-labeled dextran (RhD) to DcLNs after intra parenchymal or intra cisterna magna injections [28]. However, this group failed to detect signals in DcLNs for 3 kDa RhD after intra parenchymal or intra cisterna

magna injections. Similarly, I detected robust HF-Aβ42 signals in DcLNs at 2 hours but not in CTX (Fig. 18) [20]. My finding suggests that enhanced clearance of Aβ42 from CBL results in detection of Aβ42 in DcLNs. It is important to note that this experimental strategy seems to more authentic when I compare with normal physiological conditioned DcLNs. I am unable to explain the faint signal in DcLNs after clearance of HF-Aβ42 after72 hours later from CBL but it is important to note that fluorescent macromolecules were detectable in DcLNs after 30 min, and there was an increase in the fluorescent signal by 120 min in live animals [28].

Chapter 6

Conclusion and future perspectives

Taken together, my research indicated a potential defense mechanism against Aβ deposition in CBL. Application of this defense mechanism to CTX would prevent from AD. Aβ is still best known as a molecule to cause AD through accumulation and deposition within the frontal cortex and hippocampus in the brain that depends on rate of synthesis and clearance of Aβ. Aβ clearance or degradation rather than its synthesis have been found to be more critical in accumulation of Aβ. Therefore, Aβ clearance pathways have been emerged as a new therapeutic target for AD treatment. Although it is not fully clear about Aβ clearance but this finding will draw attention of AD scientist to find out the best possible mechanism after more investigation. Once it may possible, it would be a valid approach for developing a disease-modifying strategy to combat AD.

Chapter 7

References

[1] Blennow K, Leon MJD, Zetterberg H, Alzheimer's disease, (2006), Lancet 368: 387- 403.

[2] Grimm MOW, Mett J, Grimm HS, Hartmann T, (2017), PP Function and Lipids: A Bidirectional Link, Front. Mol. Neurosci. 10:63.

[3] Anand K, Sabbagh M, (2015), Early investigational drug targeting tau protein for the treatment of Alzheimer's Disease, Expert Opin. Investig. Drugs, 24:1355-1360.

[4] Barage SH, Sonawane KD, (2015), Amyloid cascade hypothesis: Pathogenesis and therapeutic strategies in Alzheimer's disease, Neuropeptides. 52:1-18.

[5] Selkoe DJ, Hardy J, (2016), The amyloid hypothesis of Alzheimer's disease at 25 years, EMBO Mol. Med. 8:595-608.

[6] Sun X, Chen WD, Wang YD, (2015), β-Amyloid: the key peptide in the pathogenesis of Alzheimer's disease, Front. Pharmacol. 6:221.

[7] Jonsson T, Atwal JK, Steinberg S et al., (2012), A mutation in APP protects against Alzheimer's disease and age-related cognitive decline, Nature, 488:96-99.

[8] Sevigny J, Chiao P, Bussiere T et al., (2016), The antibody aducanumab reduces Aβ plaques in Alzheimer's diease, Nature. 537:50-56.

[9] Haass C, Koo EH, Mellon A et al., (1992), Targeting of cell-surface beta-amyloid precursor protein to lysosomes: alternative processing into amyloid-bearing fragments, Nature 357:500-503.

[10] Citron M, Teplow DB, Selkoe DJ (1995), Selkoe, Generation of amyloid beta protein from its precursor is sequence specific, Neuron 14:661-670.

[11]. Funamoto S, Tagami S, Okochi M et al., (2020), Successive cleavage of β-amyloid precursor protein by γ-secretase, Semin. Cell Dev. Biol. 105:64-74.

[12] Lichtenthaler SF, (2011), α-secretase in Alzheimer's disease: molecular identity, regulation and therapeutic potential, J. neurochem. 116:10-21.

[13] Goedert M, (2015), Alzheimer's and Parkinson's diseases: The prion concept in relation to assembled Aβ, tau, and α-synuclein, Science. 349:1255555.

[14] Tomiyama T, Matsuyama S, Iso H et all., (2010), A Mouse Model of Amyloid β Oligomers: Their Contribution to Synaptic Alteration, Abnormal Tau Phosphorylation, Glial Activation, and Neuronal Loss *In Vivo*, J. Neurosci. 30:4845-4856.

[15] McMillan LE, Brown JT, Henley JM et al., (2011), Profiles of SUMO and ubiquitin conjugation in an Alzheimer's disease model, Neurosci. Lett. 502:201-208.

[16] Kakuda N, Funamoto S, Yagishita S et al., (2006), Equimolar production of amyloid beta-protein and amyloid precursor protein intracellular domain from beta-carboxyl-terminal fragment by gamma-secretase, J. Biol. Chem. 281:14776-14786.

[17] Takeda S, Sato N, Ikimura K, Nishino H et al.,(2011), Novel microdialysis method to assess neuropeptides and large molecules in free-moving mouse, Neuroscience. 186:110-119

[18] Klunk WE, Engler H, Nordberg A., et all (2004), Imaging brain amyloid in Alzheimer's disease with Pittsburgh Compound-B, Ann. Neurol. 55:306-319.

[19] Saito T, Matsuba Y, Mihira N et all., (2014), Single App knock-in mouse models of Alzheimer's disease, Nat. Neurosci. 17:661-663.

[20] Shahnur A , Masaki N, Seiki I et all., (2021), A potential defense mechanism against amyloid deposition in cerebellum, Biochem. Biophys. Res. Commun. 535:25-32.

[21] Ries M, Sastre M, (2016), Mechanisms of Aβ Clearance and Degradation by Glial Cells, Front. Aging Neurosci. 8:160.

[22] Cohen SIA, Linse S, Luheshi LM et al., (2013), Proliferation of amyloid-β42 aggregates occurs through a secondary nucleation mechanism, Proc. Natl. Acad. Sci. USA, 110:9758-63.

[23] Louveau A, Smirnov I, Keyes TJ et al., (2015), Structural and functional features of central nervous system lymphatic vessels, Nature. 523:337-341.

[24] Ahn JH, Cho H, Kim JH et al., (2019), Meningeal lymphatic vessels at the skull base drain cerebrospinal fluid, Nature. 572:62-66.

[25] Kuwabara Y, Ishizeki M, Watamura N et al., (2014), Impairments of long-term depression induction and motor coordination precede Aβ accumulation in the cerebellum of APPswe/PS1dE9 double transgenic mice, J. Neurochem. 130:432-443

[26] Uhlen M, Fagerberg L, Hallstrom BM et al., (2015), Tissue-based map of the human proteome, Science 347:6220.

[27] D. Hafez, J.Y. Huang, A.M. Huynh et al., (2011), Neprilysin-2 is an important β-amyloid degrading enzyme, Am. J. Pathol. 178:306-12.

[28] Balint L, Ocskay Z, Deak BA et., (2020), Lymph Flow Induces the Postnatal Formation of Mature and Functional Meningeal Lymphatic Vessels, Front. Immunol. 10:3043.

[29] Aspelund A, Antila S, Proulx ST et al., (2015), A dural lymphatic vascular system that drains brain interstitial fluid and macromolecules, J. Exp. Med. 212:991-999.

[30] Bradbury MW, Westrop RJ, (1983), Factors influencing exit of substances from cerebrospinal fluid into deep cervical lymph of the rabbit, J. Physiol. 339:519-534.

[31] Boulton M, Flessner M, Armstrong D et al., (1998), Determination of volumetric cerebrospinal fluid absorption into extracranial lymphatics in sheep, Am J Physiol. 274:88-96.

[32] Bradbury MW, Cole DF, (1980), The role of the lymphatic system in drainage of cerebrospinal fluid and aqueous humour, J. Physiol. 299:353-365.

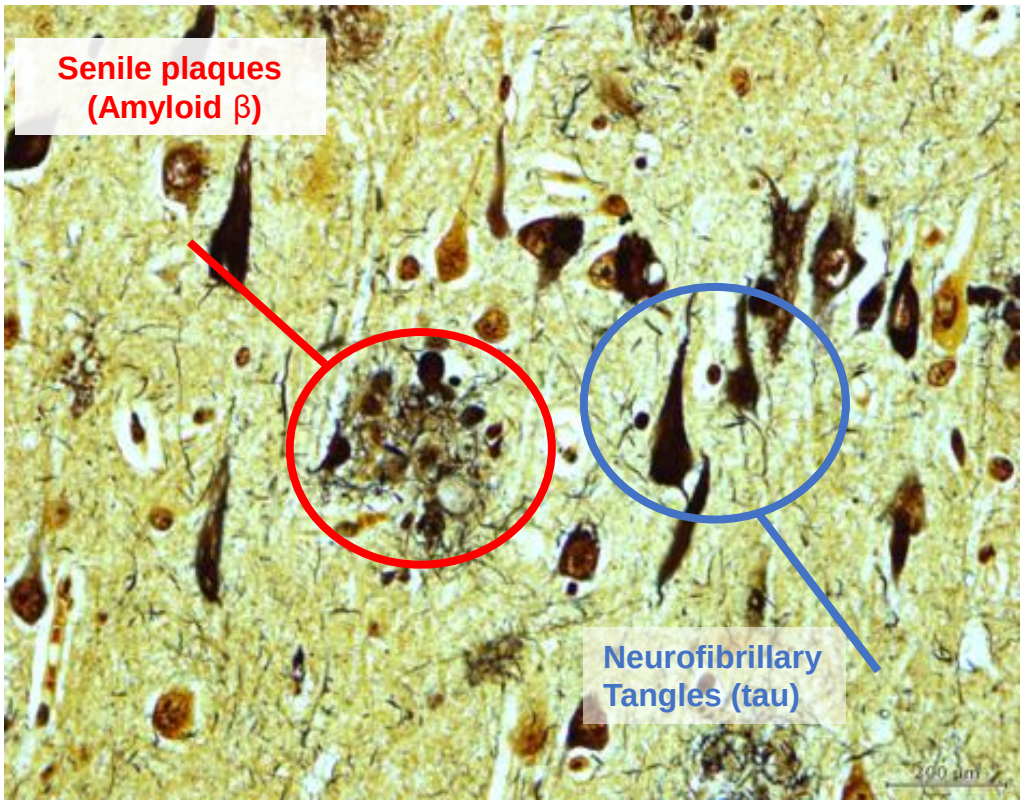

Fig. 1 Neuropathological hallmarks of AD. Bielshosky's silver staining visualizes extracellular amyloid plaques composed of amyloid-β and neurofibrillary tangles of hyperphosphorylated tau. Modified from (Blennow K et al., 2006) [1].

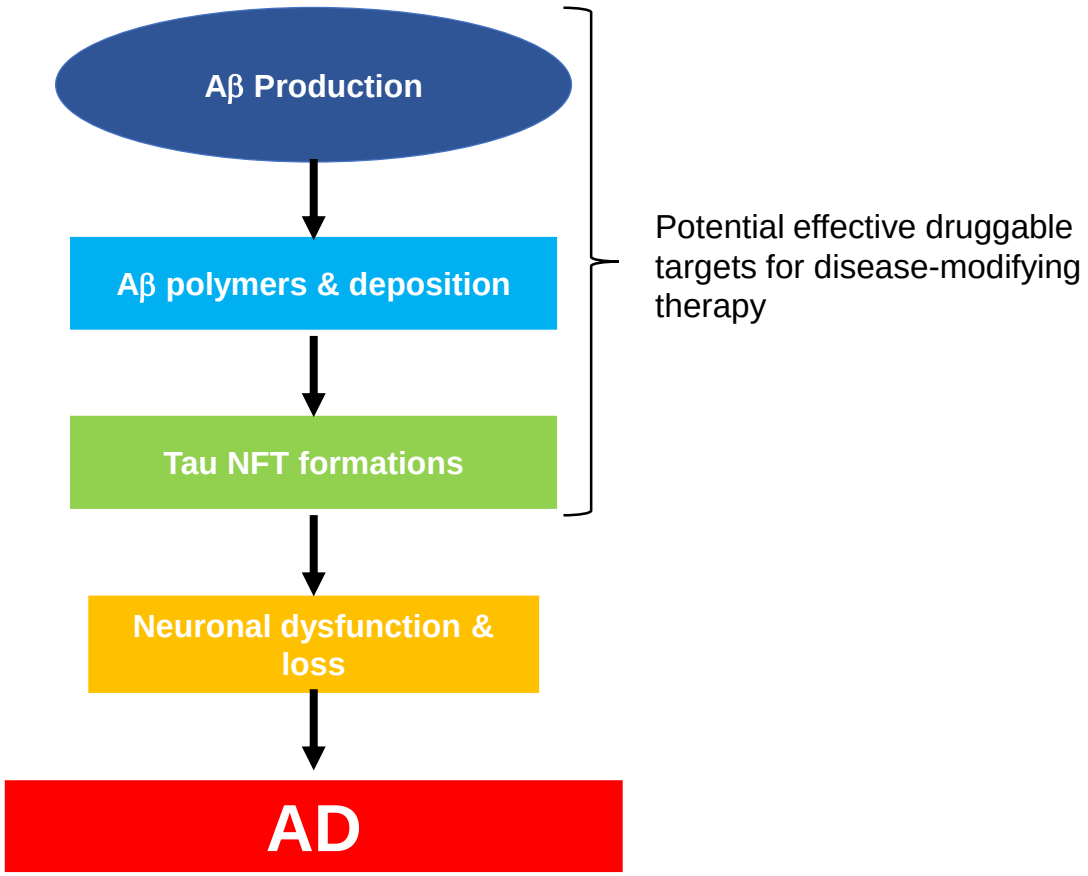

Fig. 2 The amyloid cascade hypothesis. The series of key pathogenic incidents leading to AD by the amyloid cascade hypothesis. Accumulating Aβ turns into Aβ oligomerization and gradually deposits as the forms of fibrils and senile plaques. Furthermore, Aβ aggregation alters the kinase/phosphatase activity that leads to the Tau protein hyperphosphorylated, which causes the formation of NFT; and eventual synaptic and neuronal dysfunction and AD. (Modified from San X et al., 2015)) [1].

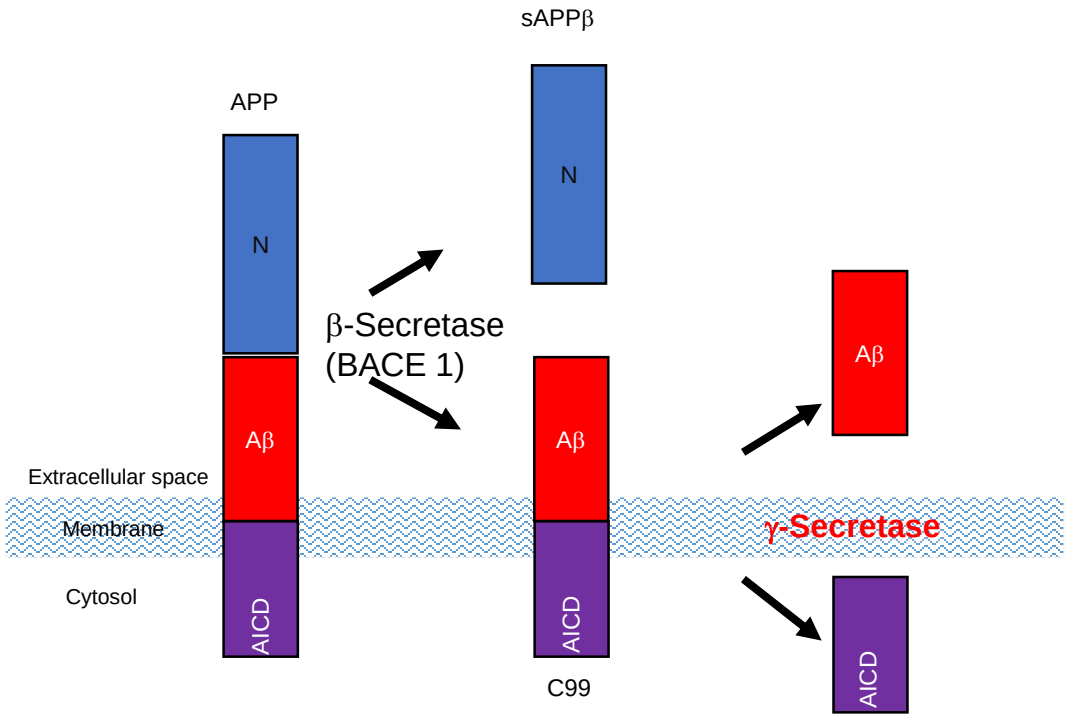

APP = Amyloid precursor protein
AICD = APP intracellular domain

Fig. 3 Generation of Aβ. In amyloidogenic pathway, APP is first cleaved byβ-secretase (BACE-1) to generate C99, the direct substrate of γ-secretase. γ-Secretase cleaves C99 in the middle of its transmembrane domain to generate extracellular Aβ and APP intracellular domain (AICD). (Modified from Lichtenthaler et al., 2011) [12].

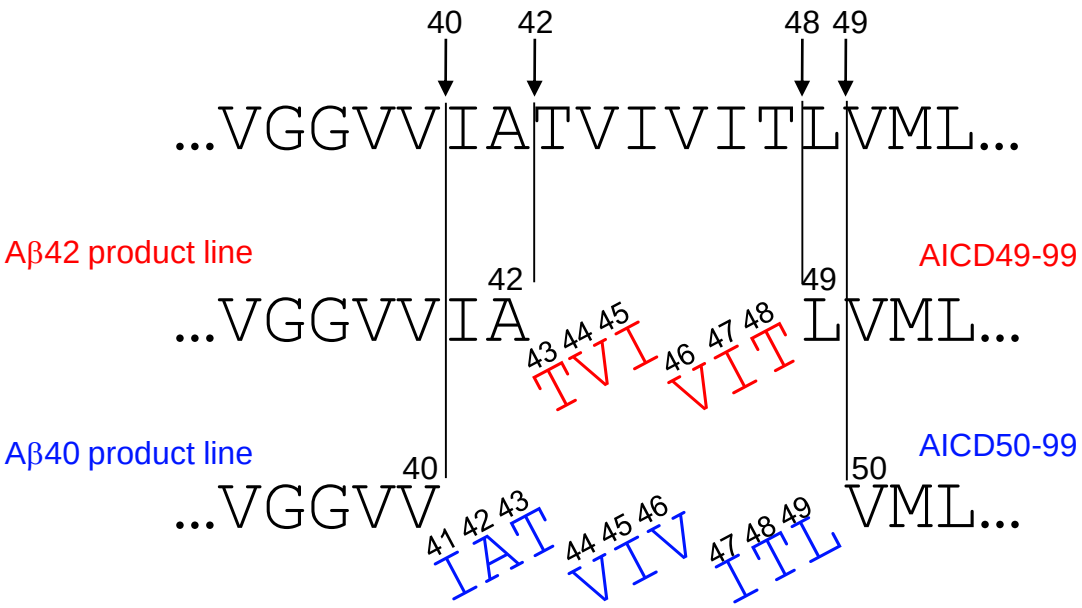

Fig. 4 Stepwise tripeptide release from C99 by γ-secretase. Cleavage at the 48th site of C99 liberates AICD49-99 and triggers the Aβ42 product line by successively releasing the tripeptides VIT and TVI. Cleavage at the 49th site leads to AICD50-99 production and the Aβ40 product line by releasing ITL, VIV, and IAT. Modified from Funamoto S et al., 2020 [11].

a

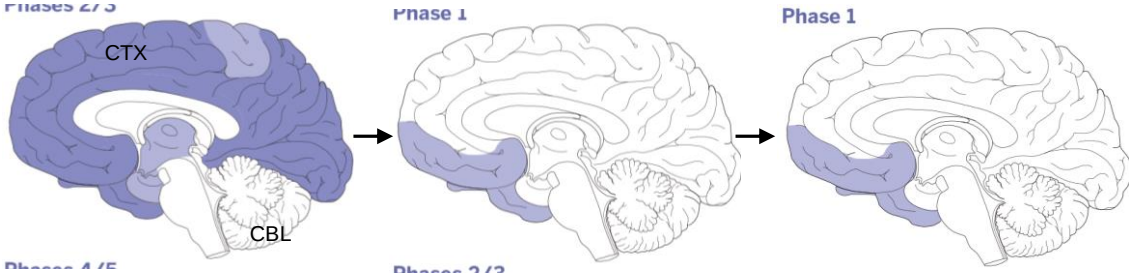

b

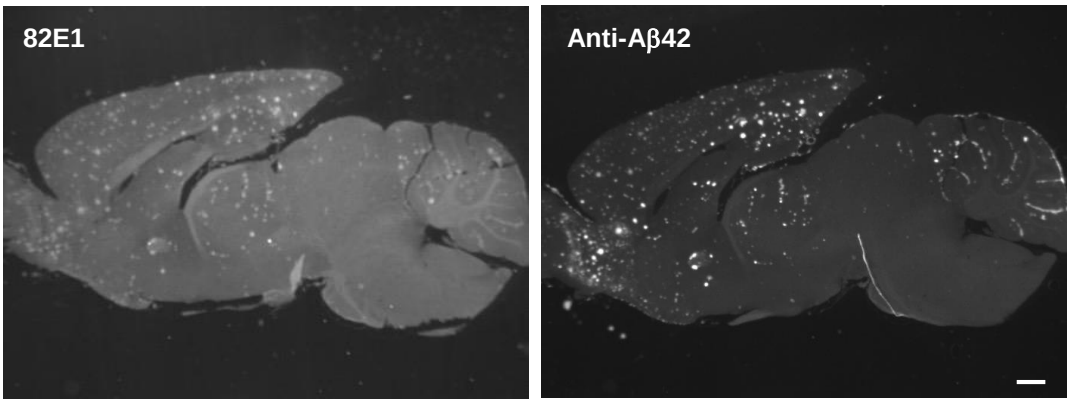

Fig. 5 Aβ deposition in brain. (**a**) In human, Aβ plaques (blue) develop first in the neocortex at early stage. In severe cases of AD, Aβ plaques found in CBL. Modified from Godert M et all., 2015 [13]. (**b**) Immunofluorescent double-staining with 82E1 and anti-Aβ42 antibodies showed less Aβ deposition in CBL than CTX in both 12-month tg2576 mice. Scale bar indicates 1 mm.

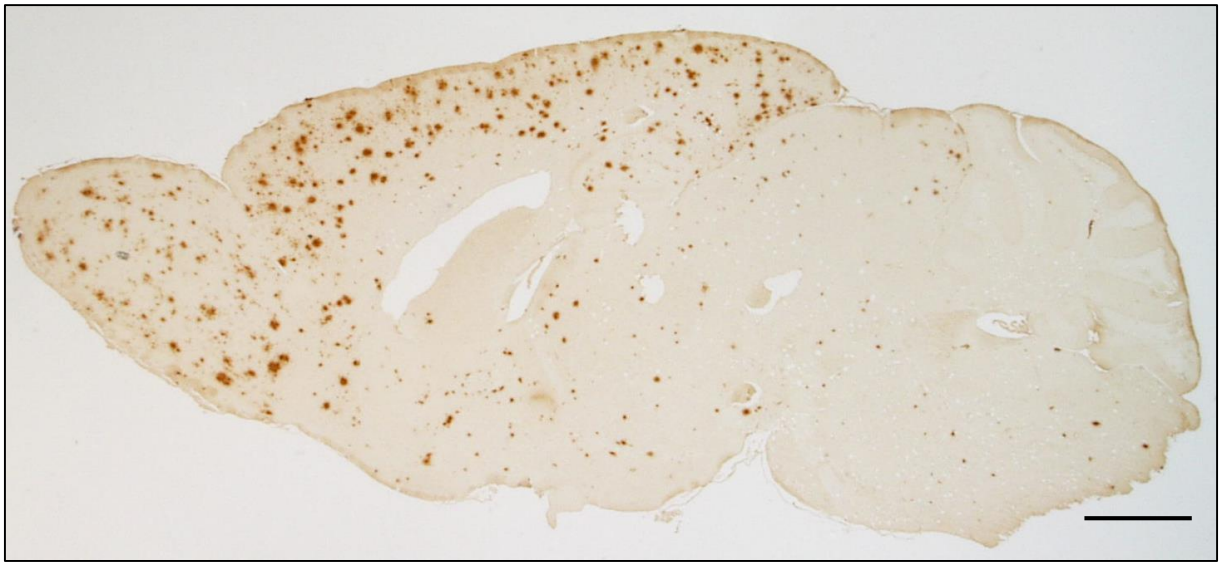

Fig. 6 Less Aβ burden in CBL of *APP^{NL-G-F}*. *APP^{NL-G-F}* is an AD model mice in which aggregation prone Aβ42 is produced predominantly in whole brain. Importantly, the DAB immunohistochemistry staining with anti-Aβ (6E10) showed less Aβ deposit in CBL of 3-month old *APP^{NL-G-F}* mice than CTX that is similar with human brain. Scale bar indicate (1mm). (Shahnur A et al., 2021) [20].

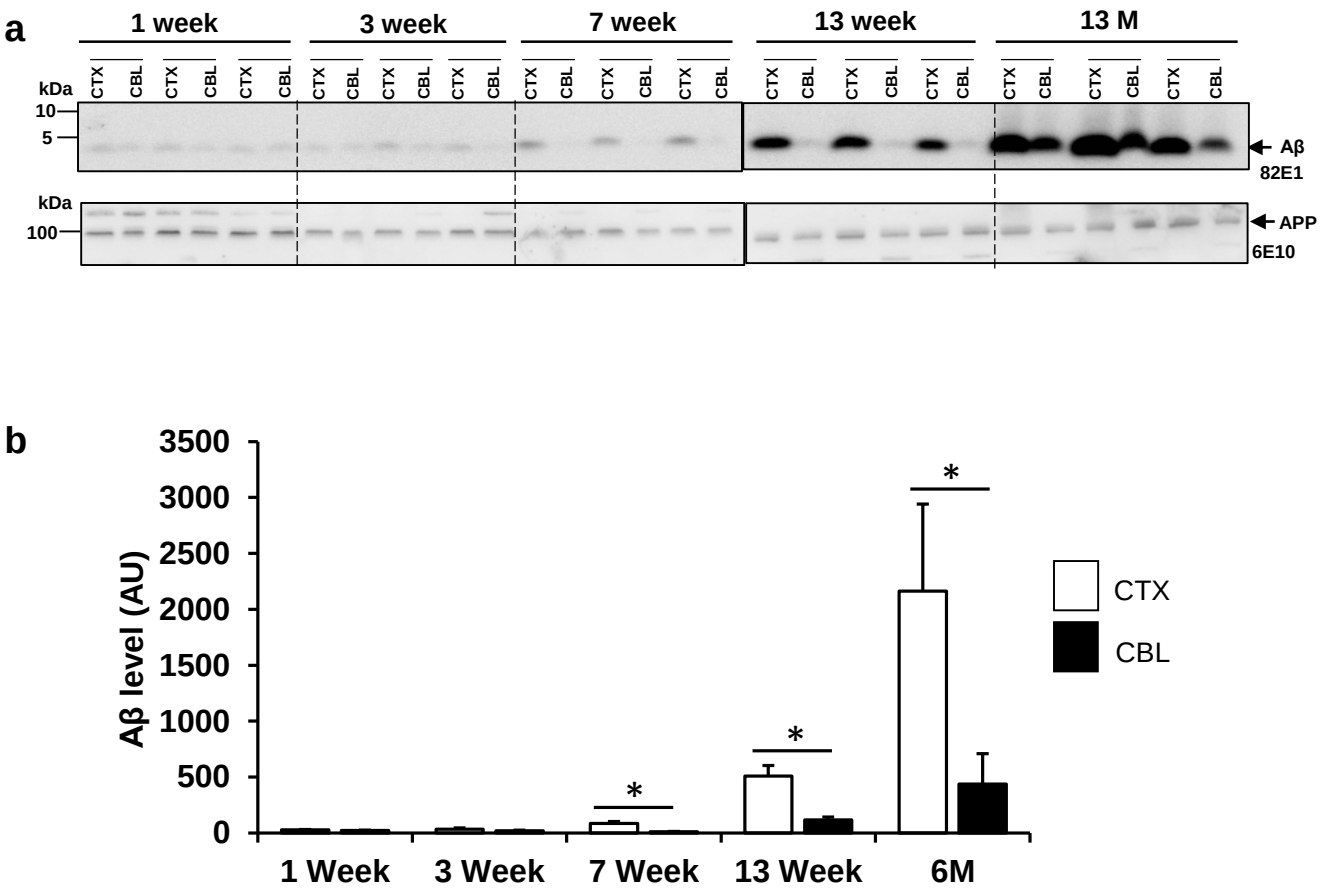

Fig. 7 Aβ in CTX and CBL. (**a**) TS soluble and insoluble fractions from CTX and CBL in *APP*$^{NL\text{-}G\text{-}F}$ mice were subjected to immunoprecipitation with 4G8 antibody and western blotting with 82E1 antibody for Aβ detection. (**b**) No difference on Aβ levels between CTX and CBL in 1- and 3-week mice, however the level Aβ in CTX of 6-month old mice was 4.5 times higher than that in CBL. APP expression levels were consistent in CTX and CBL in all mice tested. Data represent mean ± SD. n = 3 mice per group. * $p < 0.05$ (paired *t*-test). (Shahnur A et al., 2021) [20].

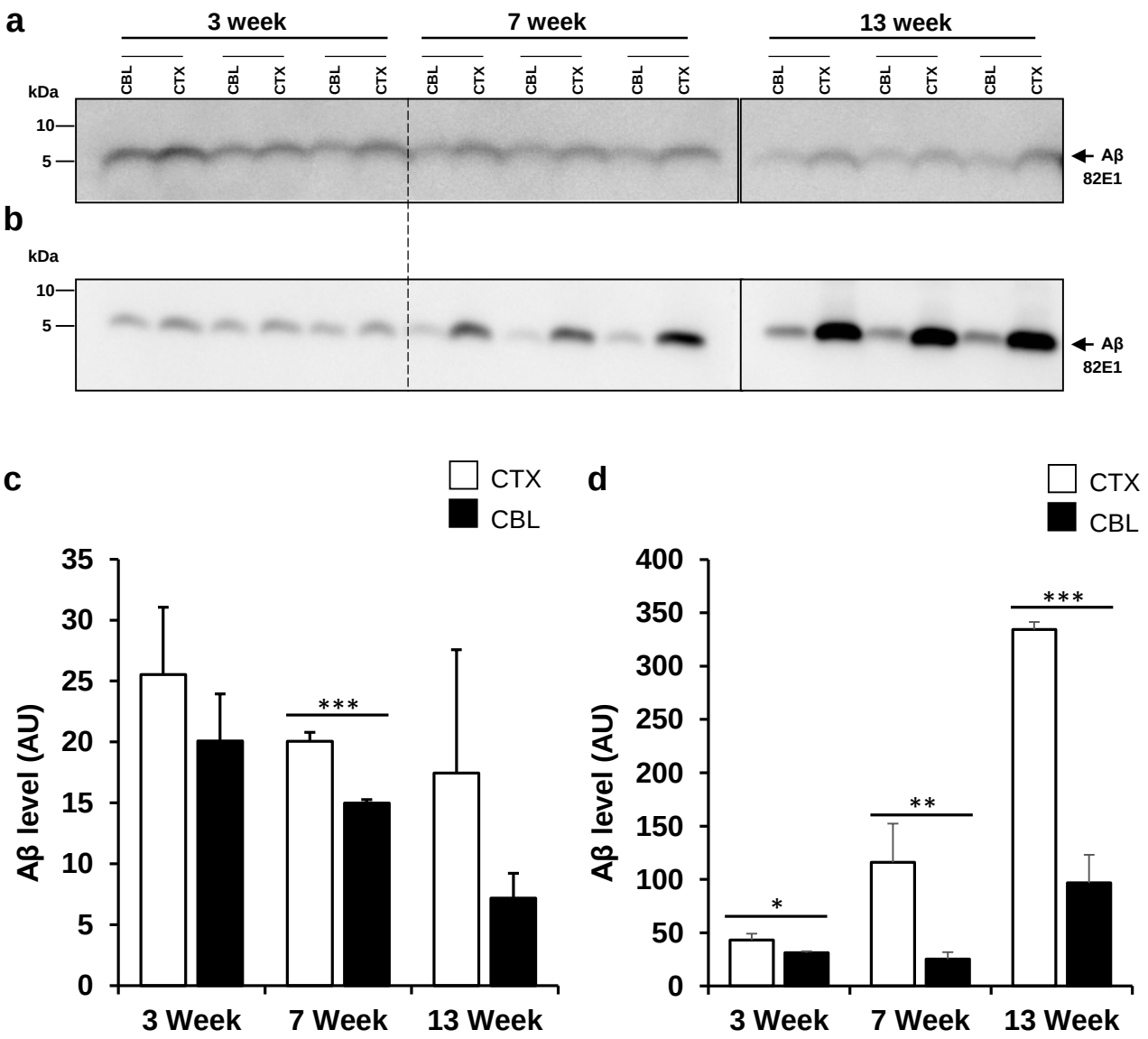

Fig. 8 Soluble and insoluble Aβ in CTX and CBL. (**a**) TS soluble and (**b**) TS insoluble fractions from CTX and CBL in *APP*$^{NL\text{-}G\text{-}F}$ mice were subjected to immunoprecipitation with 4G8 antibody and western blotting with 82E1 antibody for Aβ detection. (**c**) Less difference on Aβ levels between CTX and CBL in 3- , 7- and 13-week mice in TS soluble fraction. (**d**) Difference on Aβ levels between CTX and CBL in 3- , 7- and 13-week mice in TS insoluble fraction was enhanced. Data represent mean ± SD. n = 3 mice per group. * $p < 0.05$. ** $p < 0.01$. *** $P < 0.001$ (paired *t*-test).

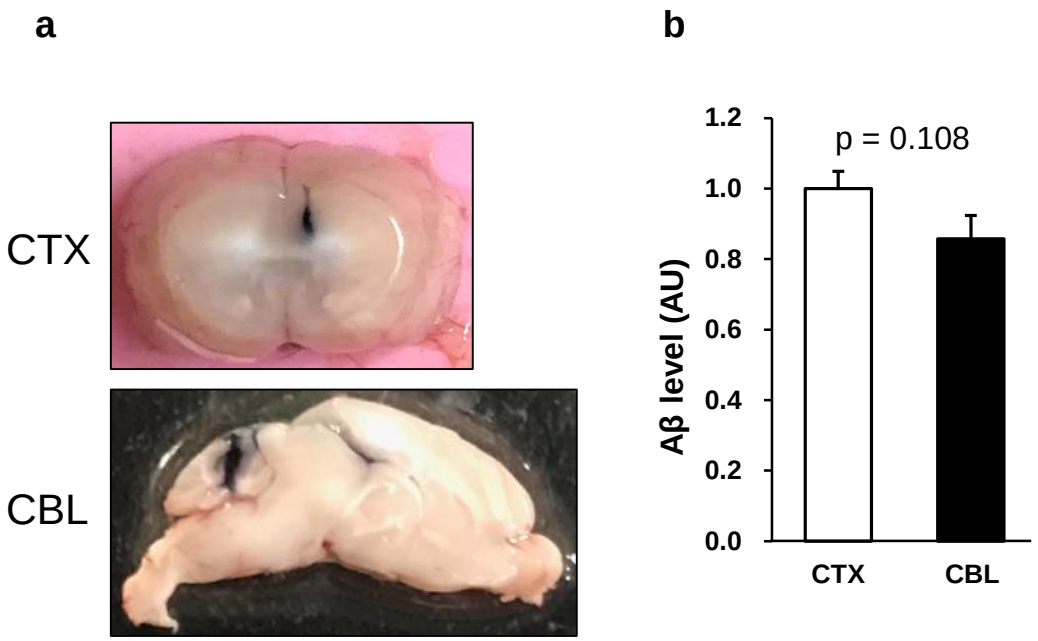

Fig. 9 ISF Aβ level in CTX and CBL. (**a**) Representative image of probe insertion sites in CTX and CBL for microdialysis. (**b**) ISF Aβ level between CTX and CBL in 4-month old $APP^{NL\text{-}G\text{-}F}$ mice. No Significant difference was observed between them. Data represent mean ± SD. n = 4 mice per group. p = 0.108 (paired *t*-test). Courtesy of Dr. M. Nakano. (Shahnur A et al., 2021) [20].

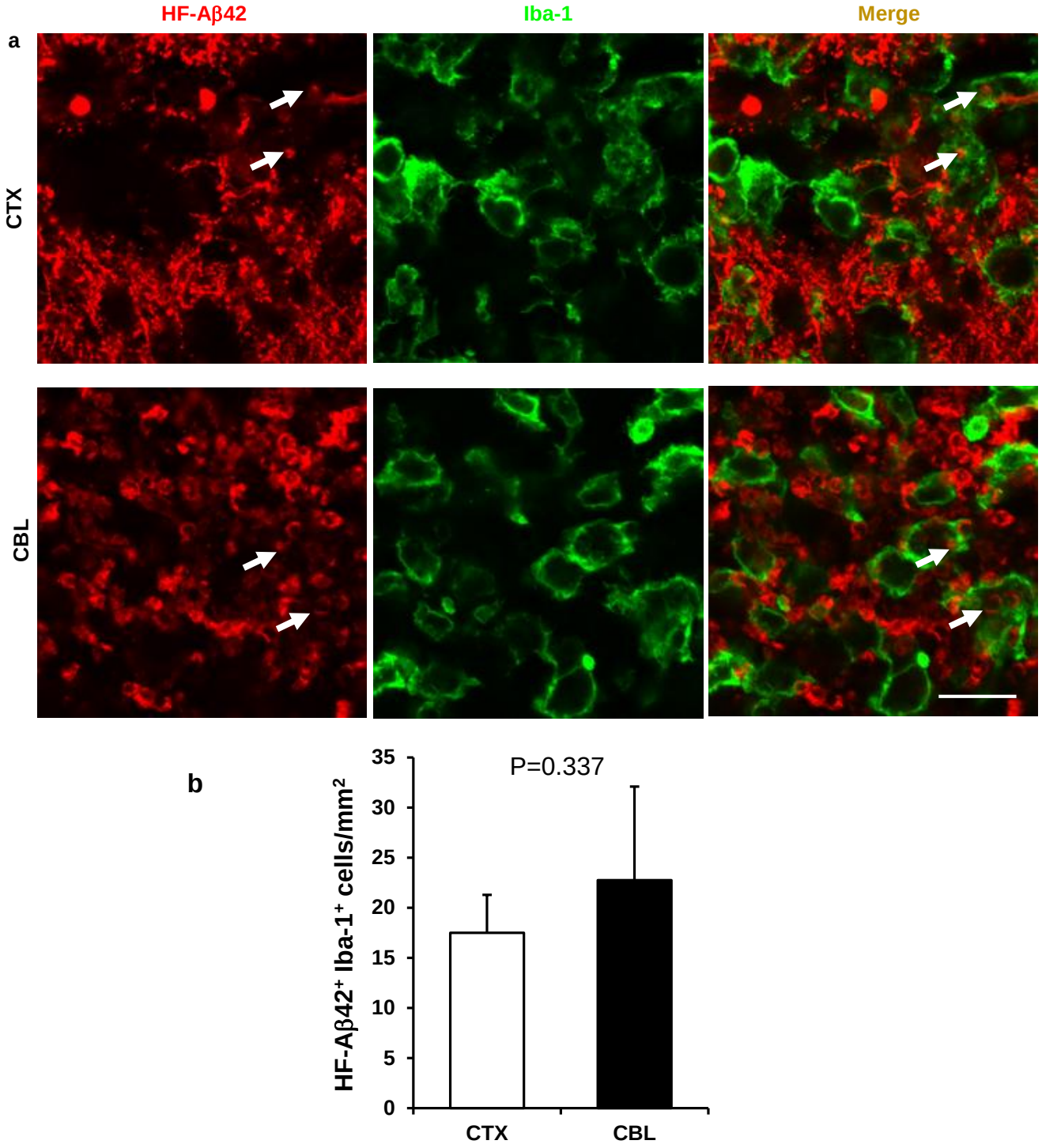

Fig. 10 Microglial engulfment of Aβ. (**a**) HiLyte™ Fluor 555 labeled Aβ1-42 (HF-Aβ42) was injected into CTX and CBL of 8-week mice and observed its localization with Iba-1 positive cells after 72 hours of the injection. Arrows indicate positions of HF-Aβ in Iba-1 positive microglia cells. Scale bar indicates 20 μm. (**b**) Density of HF-Aβ42 and Iba-1 positive cells in CTX and CBL. Data represent mean ± SD. n = 4 mice per group. p = 0.33 (paired *t*-test). (Shahnur A et al., 2021) [20].

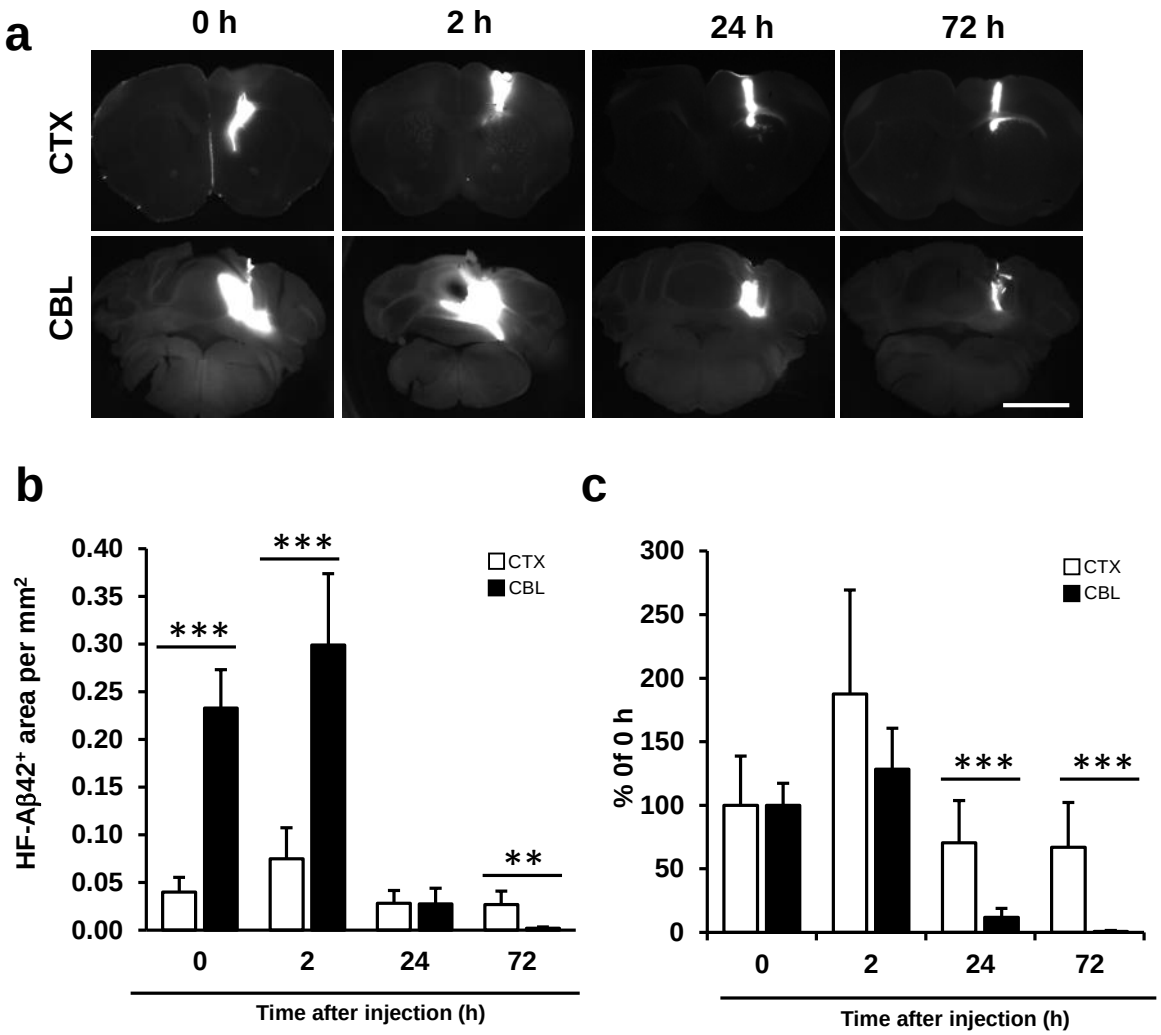

Fig. 11 HF-Aβ42 diffusion in brain tissues at low concentration. HF-Aβ42 was stereotaxically injected into the brain parenchyma. (**a**) Representative coronal sections of C57BL6 mouse brains injected with HF-Aβ42 at 0.5mg/ml conc. (**b**) Quantification of HF-Aβ42 positive areas in CBL and CTX at the time indicated. HF-Aβ42 positive areas in CBL expanded around six-times than that in CTX right after injection (0 h). Importantly, the HF-Aβ42 positive area decreased sharply after 24 hours. In contrast, HF-Aβ42 positive areas in CTX tended to be constant up to 72 h. (**c**) Normalization with 0 h indicate that diffusion rate is higher in CBL than CTX after 24 h. Scale bar indicates 2 mm. Data represent mean ± SD. n = 3~5 mice per group. ** $p < 0.01$. *** $P< 0.001$ (unpaired *t*-test). (Shahnur A et al., 2021) [20].

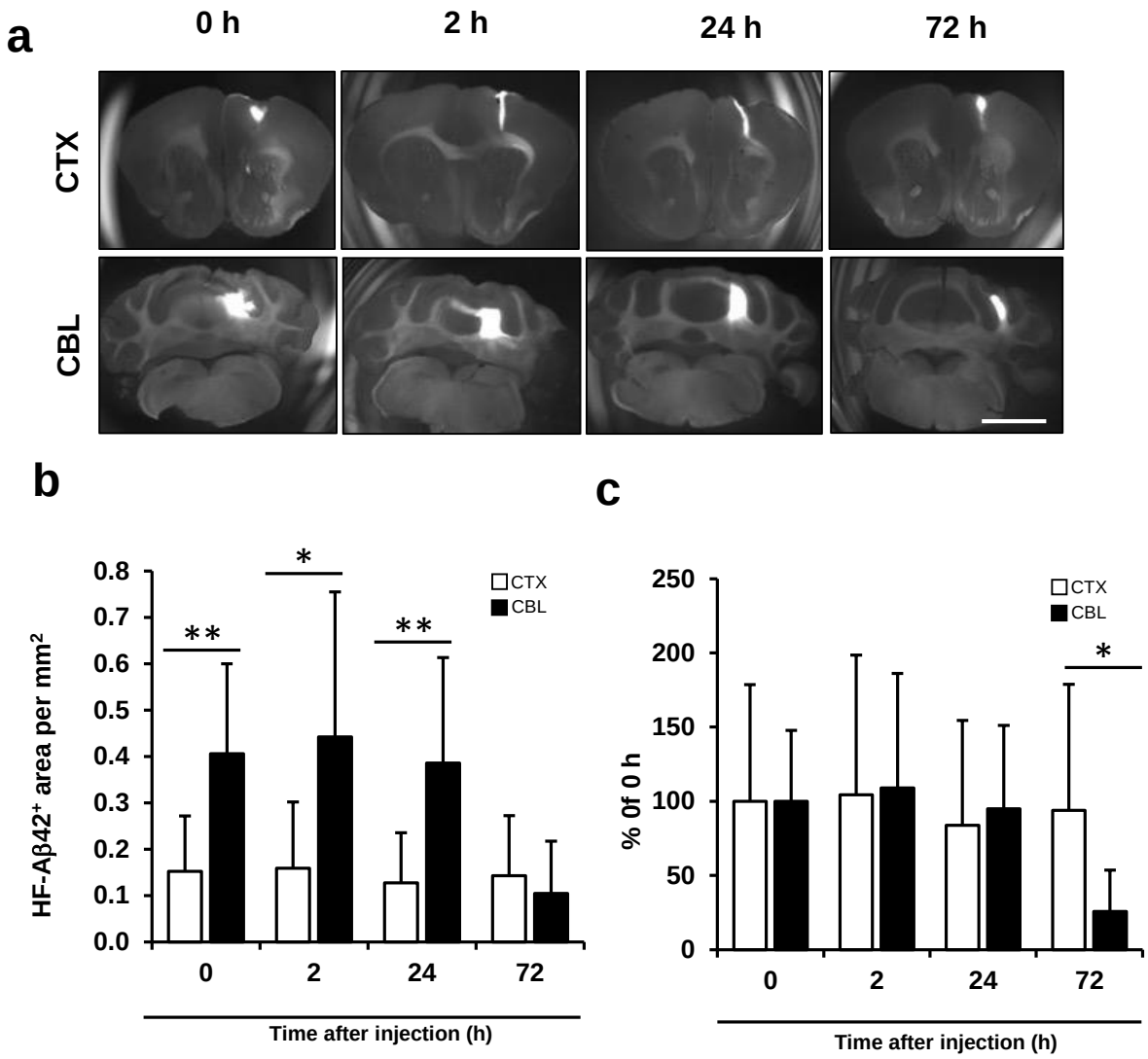

Fig. 12 HF-Aβ42 diffusion in brain tissues at high concentration. HF-Aβ42 was stereotaxically injected into the brain parenchyma. (**a**) Representative coronal sections of C57BL6 mouse brains injected with HF-Aβ42 at 2mg/ml conc. (**b)** Quantification of HF-Aβ42 positive areas in CBL and CTX at the time indicated. HF-Aβ42 positive areas in CBL expanded around four-times than that in CTX right after injection (0 h). Importantly, the HF-Aβ42 positive area decreased sharply after 72 hours. In contrast, HF-Aβ42 positive areas in CTX was tended to be constant up to 72 hours. (**f**) Normalization with 0-h indicate that diffusion rate is higher in CBL than CTX after 72 h Scale bar indicates 2 mm. Data represent mean ± SD. n = 7~10 mice per group. * $p < 0.05$.** $p < 0.01$. (unpaired *t*-test).

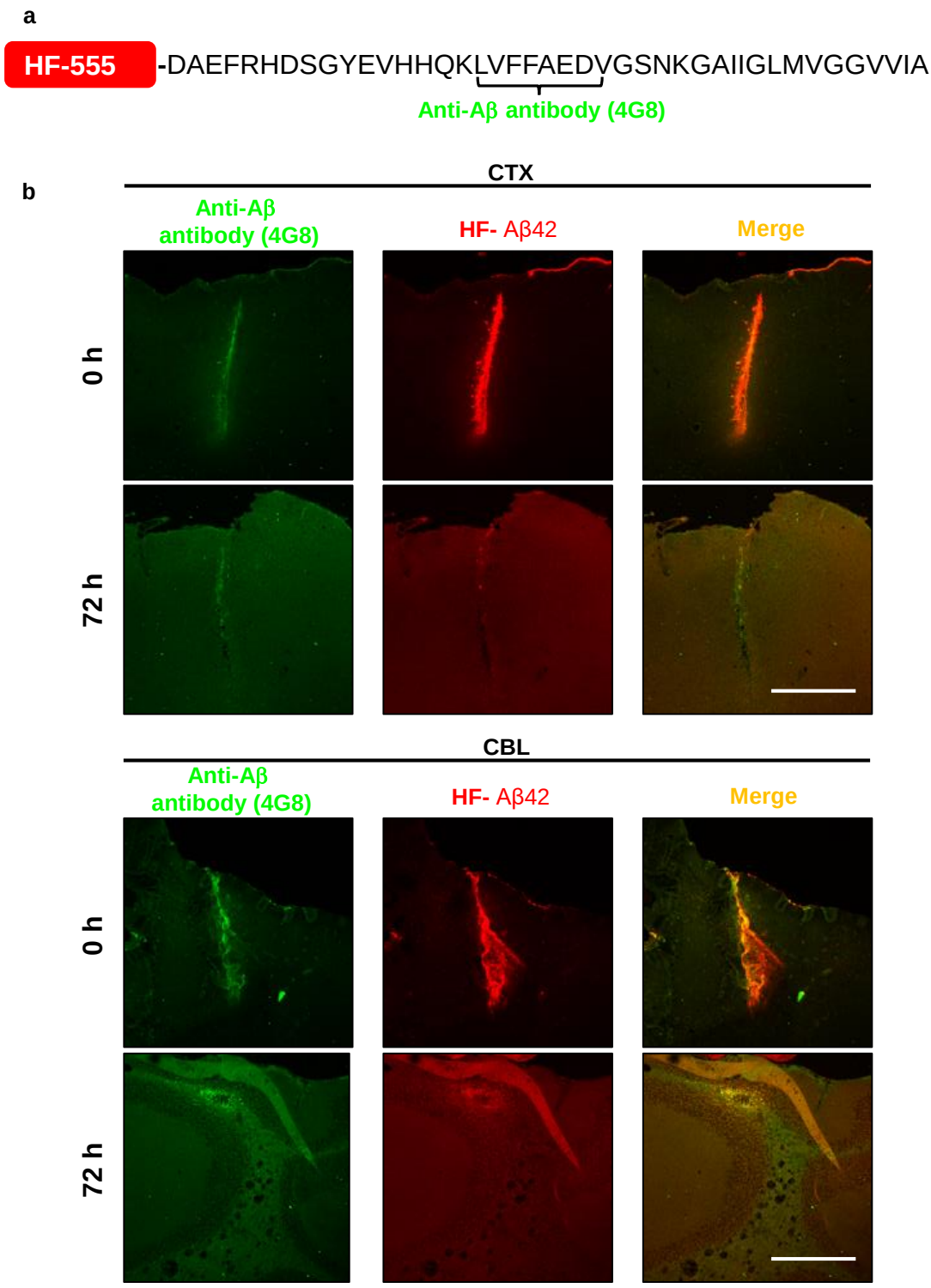

Fig. 13 Immunological detection of HF-Aβ42 in brain tissues. (**a**) Hilyte Fluor-555 labeled Aβ42 sequence that can recognize anti-Aβ (4G8) at 17-24 amino acid. (**b**) Immunostaining demonstrated 4G8 (green), HF-Aβ42 (red) and Merge (yellow) staining. Top panel for CTX and bottom panel for CBL. Scale bar indicates 500 μm.

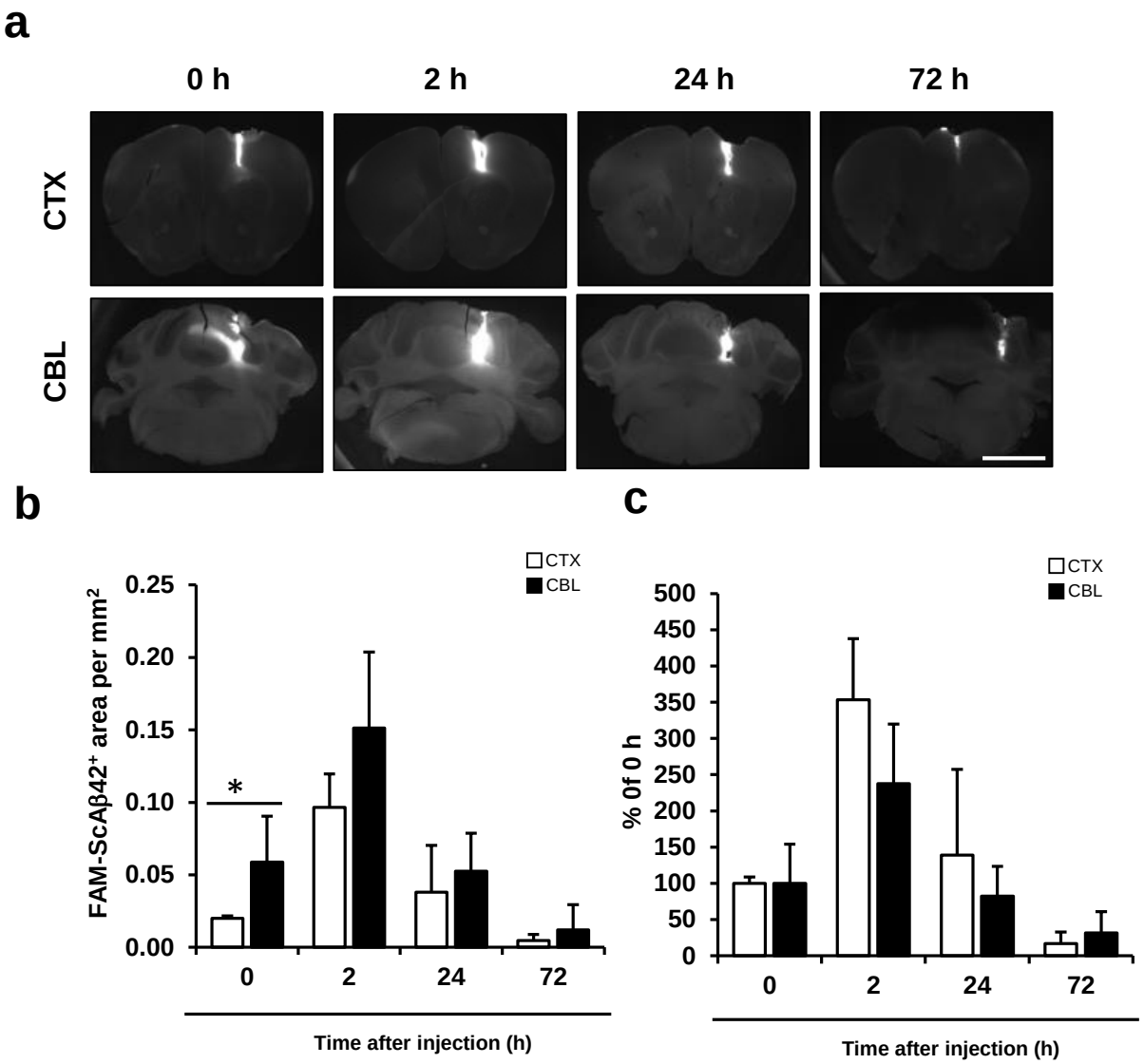

Fig. 14 FAM-scAβ42 diffusion in brain tissues. FAM-scAβ42 was stereotaxically injected into the brain parenchyma. (**a**) Representative coronal sections of C57BL6 mouse brains injected with FAM-scAβ42. (**b**) Quantification of FAM-scAβ42 positive areas at the time indicated. FAM-scAβ42 positive areas in CBL was 2.5-times larger than that in CTX at right after injection (0 h). FAM-scAβ42 positive areas reached to the maximum level at 2 hours both in CTX and CBL. Importantly, we detected no significant difference in the FAM-scAβ42 positive area between CTX and CBL after 2 hours of injection. (**c**) Normalization with 0-h indicate that diffusion rate is simlar in CTX and CBL untill 72 h. Scale bar indicates 2 mm. Data represent mean ± SD. n=5~6 mice per group. *, $p < 0.05$ (unpaired *t*-test). (Shahnur A et al., 2021) [20].

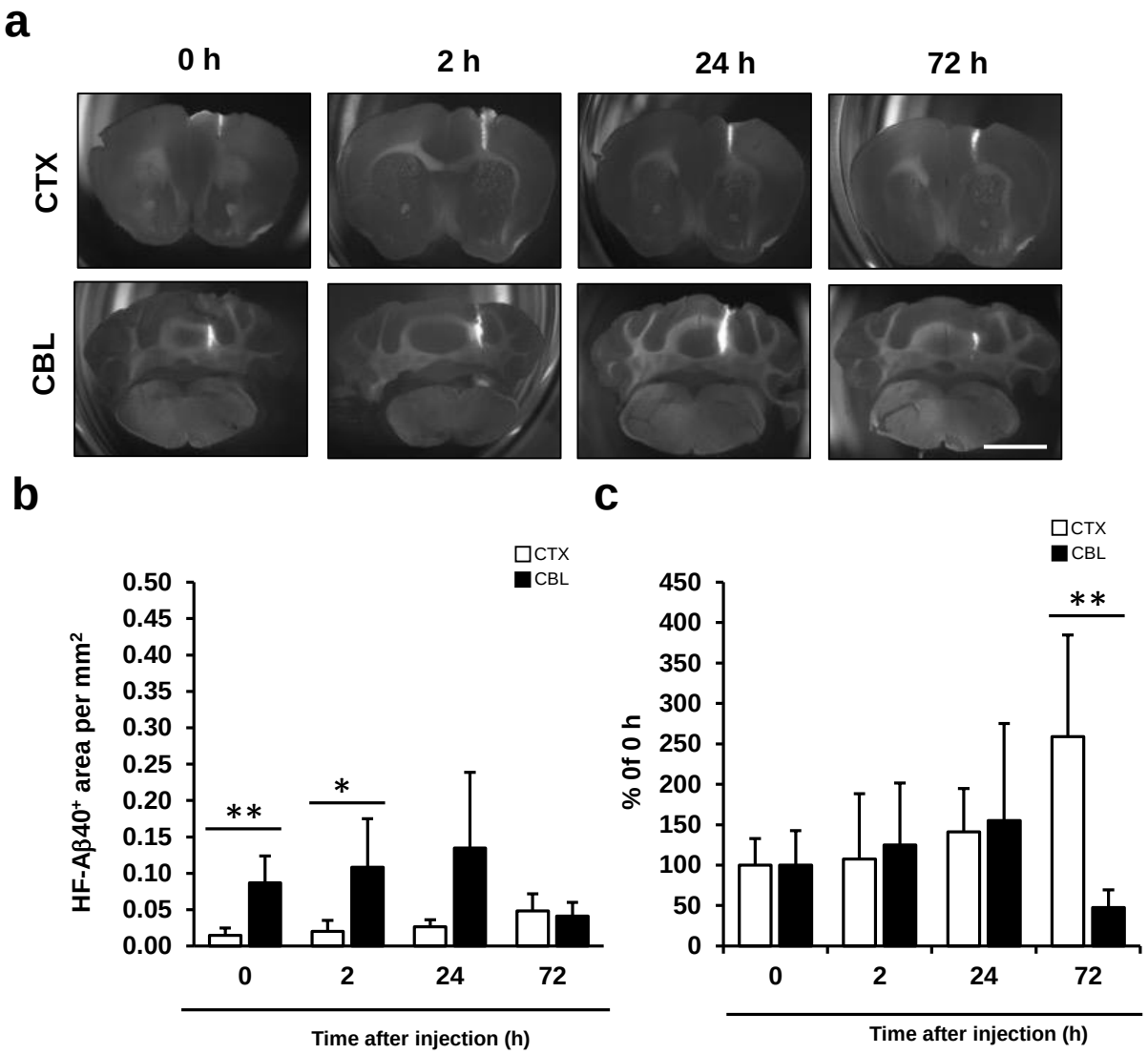

Fig. 15 HF-Aβ40 diffusion in brain tissues. HF-Aβ40 was stereotaxically injected into the brain parenchyma. (**a**) Representative coronal sections of C57BL6 mouse brains injected with HF-Aβ40 at 2mg/ml concentration. (**b**) Quantification of HF-Aβ42 positive areas in CBL and CTX at the time indicated. HF-Aβ40 positive areas in CBL expanded around four-times than that in CTX right after injection (0 h). HF-Aβ40 positive areas reached to the maximum level at 24 hours both in CTX and CBL. (**c**) Normalization with 0-h indicate that diffusion rate is higher in CBL than CTX after 72 h. Scale bar indicates 2 mm. Data represent means ± SD, n= 4 ~5 per group, * $P < 0.05$, ** $P < 0.01$ (unpaired *t*-test).

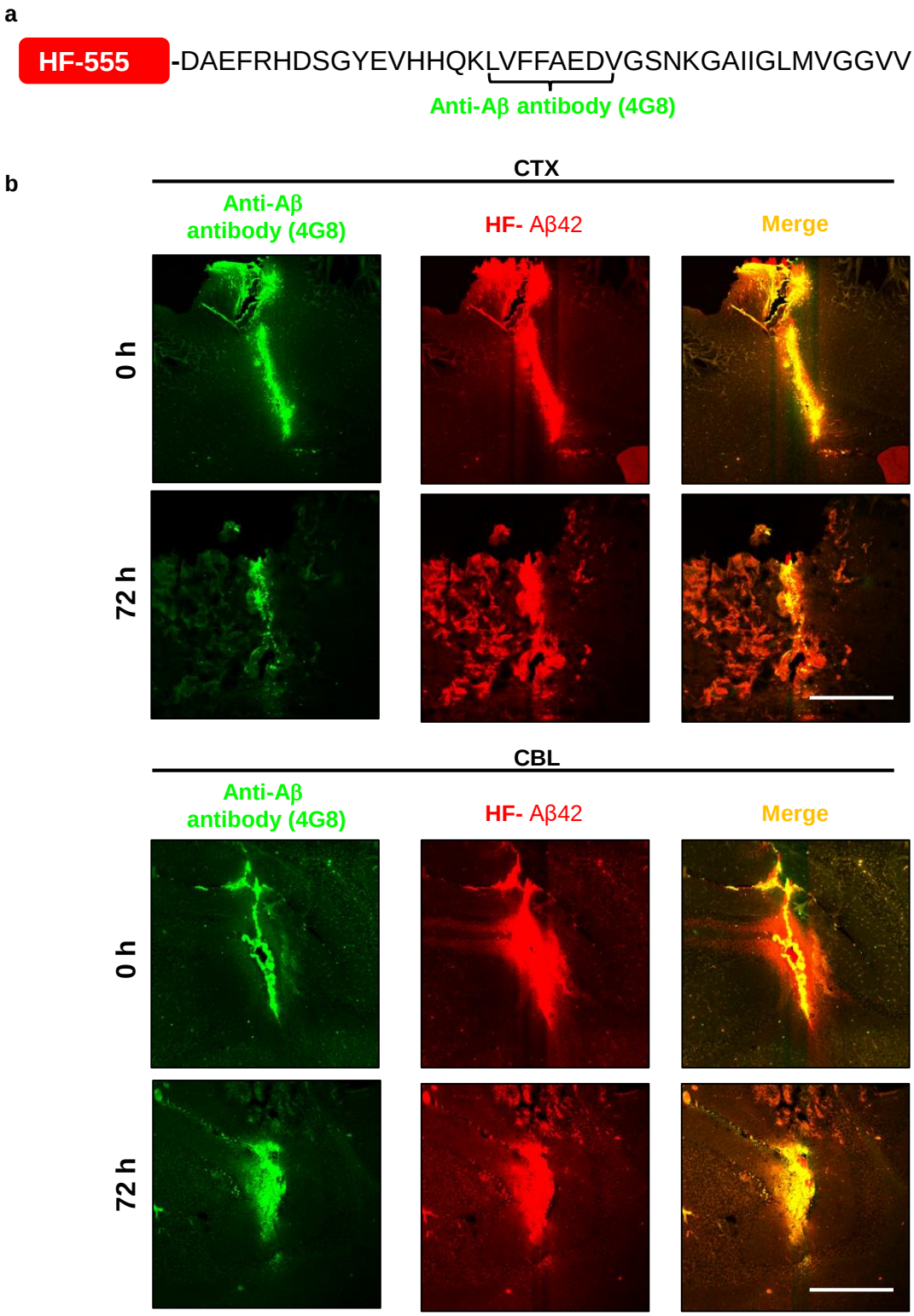

Fig. 16 Immunological detection of HF-Aβ40 in brain tissues. (**a**) Hilyte Fluor-555 labeled Aβ40 sequence that can recognize anti-Aβ (4G8) at 17-24 amino acid. (**b**) Immunostaining demonstrated 4G8 (green), HF-Aβ40 (red) and Merge (yellow) staining. Top panel for CTX and bottom panel for CBL. Scale bar indicates 500 μm.

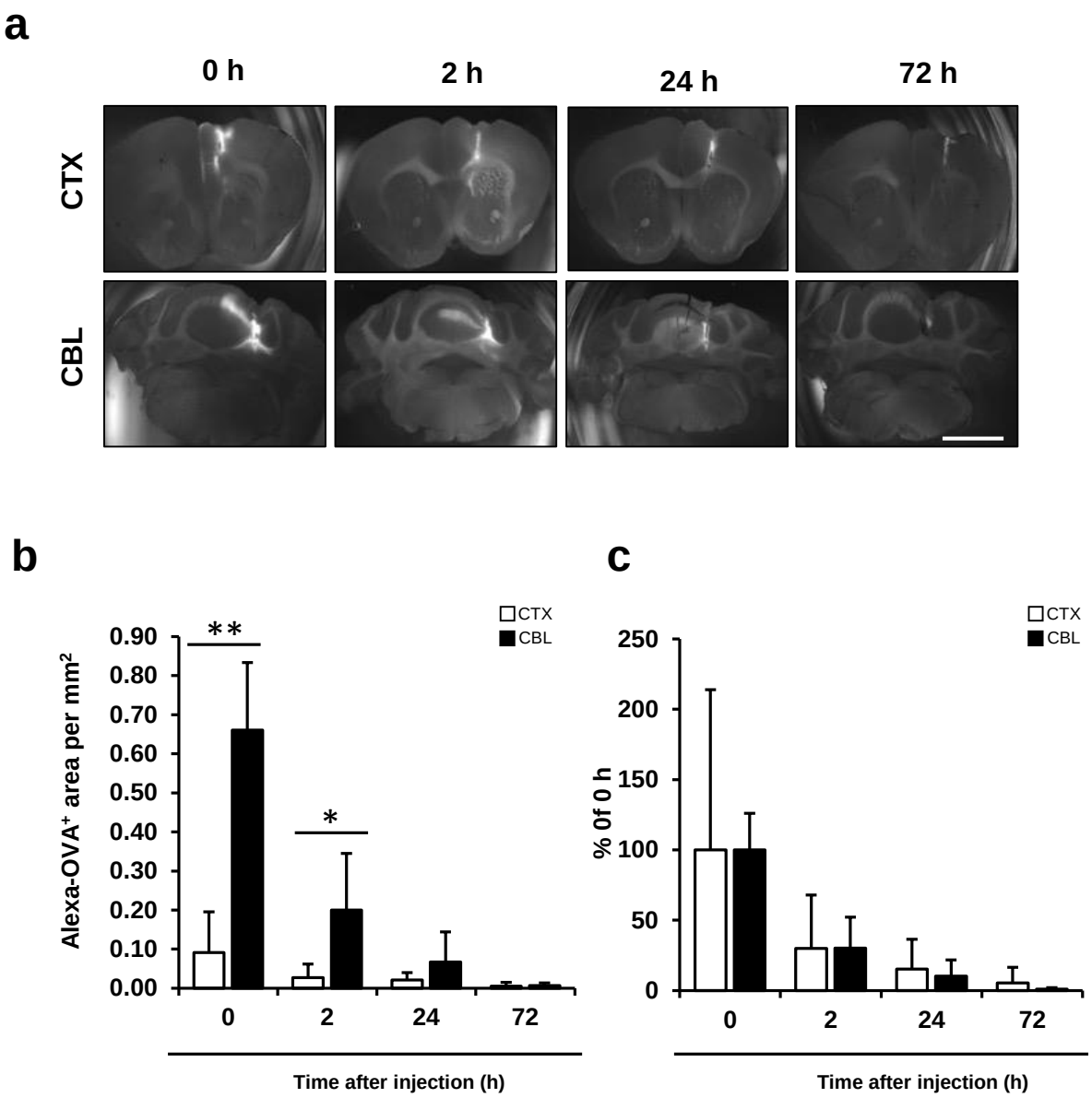

Fig. 17 Alexa-OV diffusion in brain tissues. Alexa-OV was stereotaxically injected into the brain parenchyma. (**a**) Representative coronal sections of C57BL6 mouse brains injected with Alexa-OV at 2mg/ml concentration. (**b**) Quantification of Alexa-OV positive areas at the time indicated. Alexa-OV in CBL was 6-times larger than that in CTX right after injection (0 h). Importantly, Alexa-OV positive areas in CTX and CBL decreased similarly after 2 hours of injection. (**c**) Normalization with 0-h indicate that diffusion rate is higher in CBL than CTX after 72 h. Scale bar indicates 2 mm. Data represent mean ± SD. n = 3~5 mice per group. *, $p < 0.05$. **, $p < 0.01$ (unpaired *t*-test). (Shahnur A et al., 2021) [20].

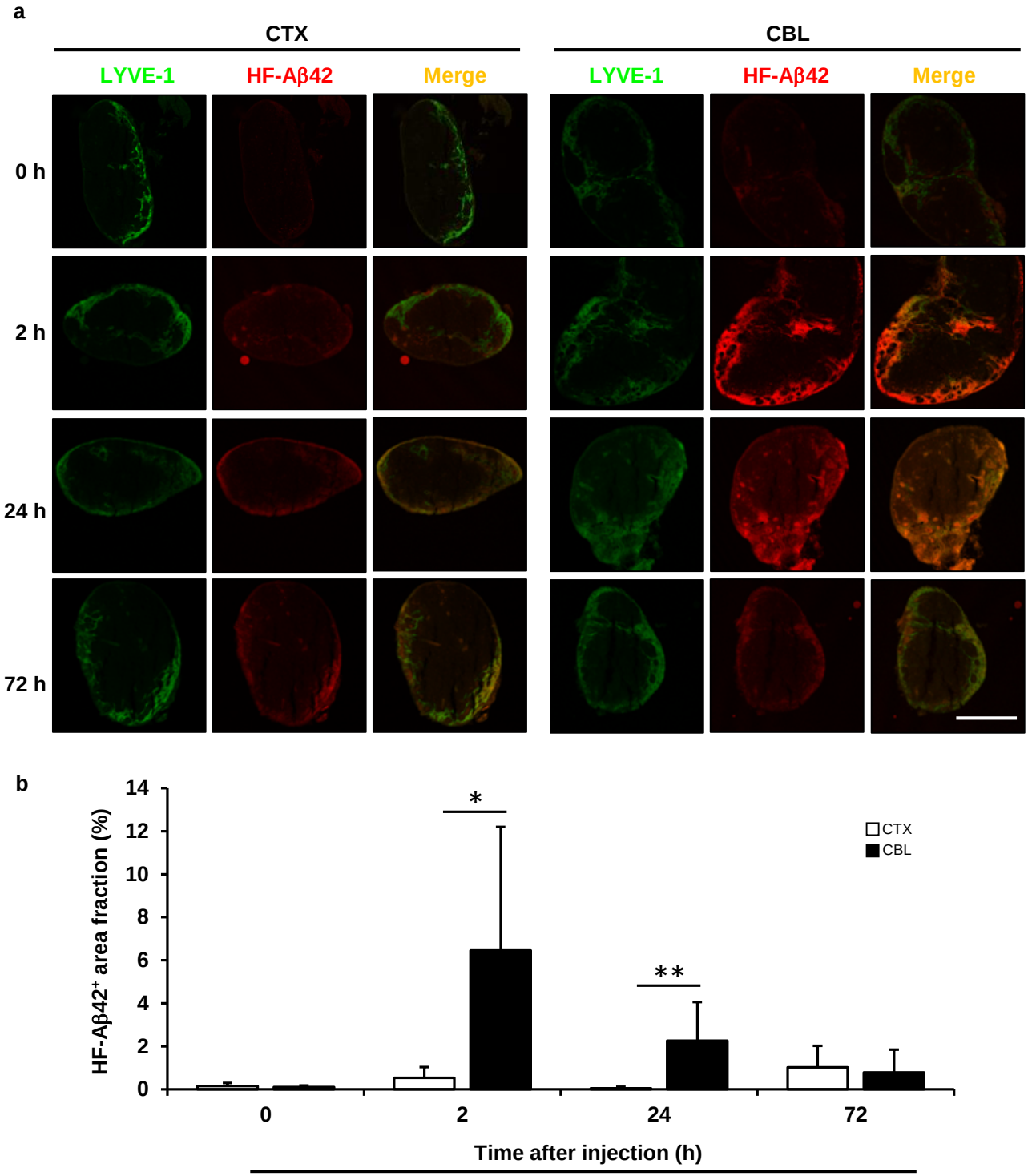

Fig. 18 Drainage of HF-Aβ42 from brain tissues into DcLNs. (**a**) Detection of brain-injected HF-Aβ42 in Dclns. Dclns were removed in each tome point after HF-Aβ42 injection in CTX (left panel) and CBL (right panel). We detected robust HF-Aβ42 signals in DcLNs in 2 and 24 hours after CBL injection. HF-Aβ42 (red), LYVE-1 (green), and Merge (yellow). Scale bar indicates 500 μm. (**b**) Quantification for HF-Aβ42 positive area fraction in DcLns sections. HF-Aβ42 positive area fraction in DcLNs of CBL injection reached at the maximum level at 2 hours and decreased over time, while that of CTX was faint. Data represent mean ± SD. n = 7~10 mice per group. *, $p < 0.05$. **, $p < 0.01$ (unpaired *t*-test). (Shahnur A et al., 2021) [20].

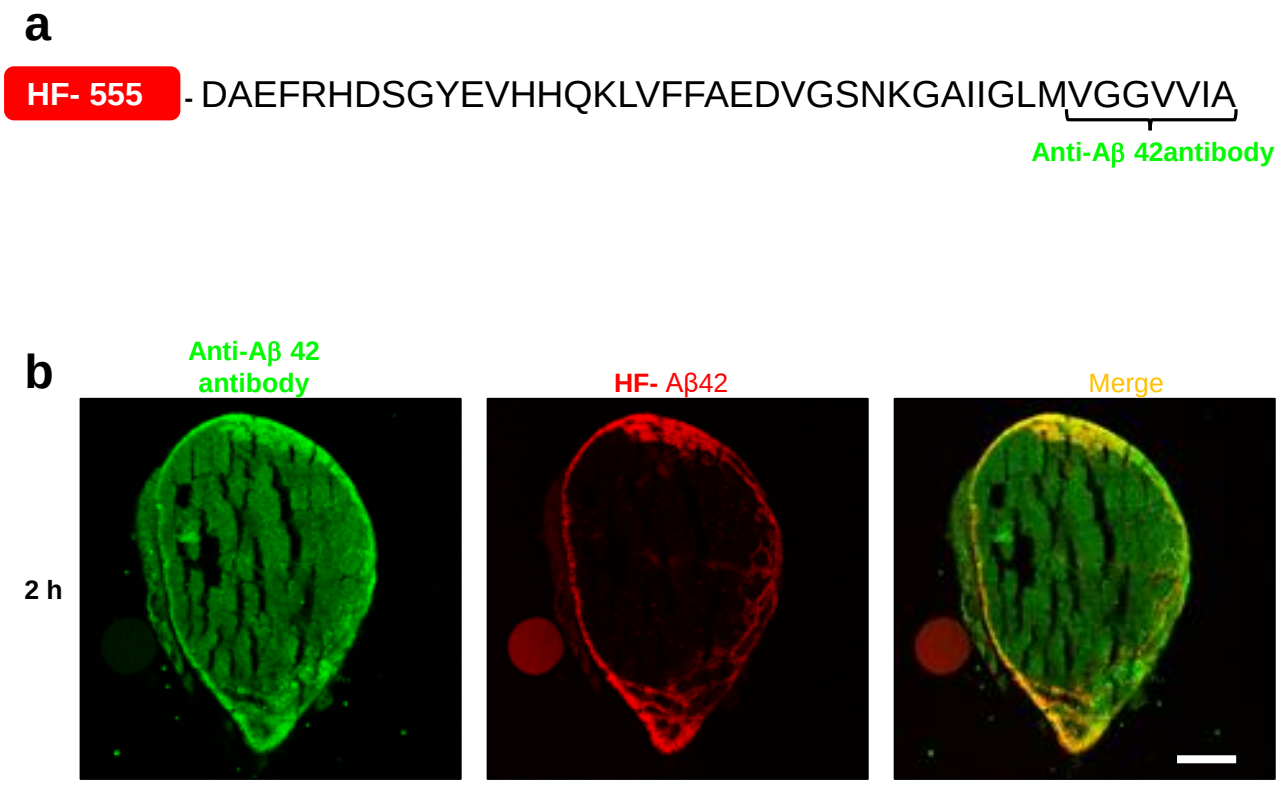

Fig. 19 Immunological detection of HF-Aβ42 in DcLNs. (**a**) Hilyte Fluor-555 labeled Aβ42 sequence that can recognize anti-Aβ42 antibody. (**b**) Immunostaining demonstrated anti-Aβ42 (green), HF-Aβ42 (red) and Merge (yellow). Scale bar indicates 200 μm.

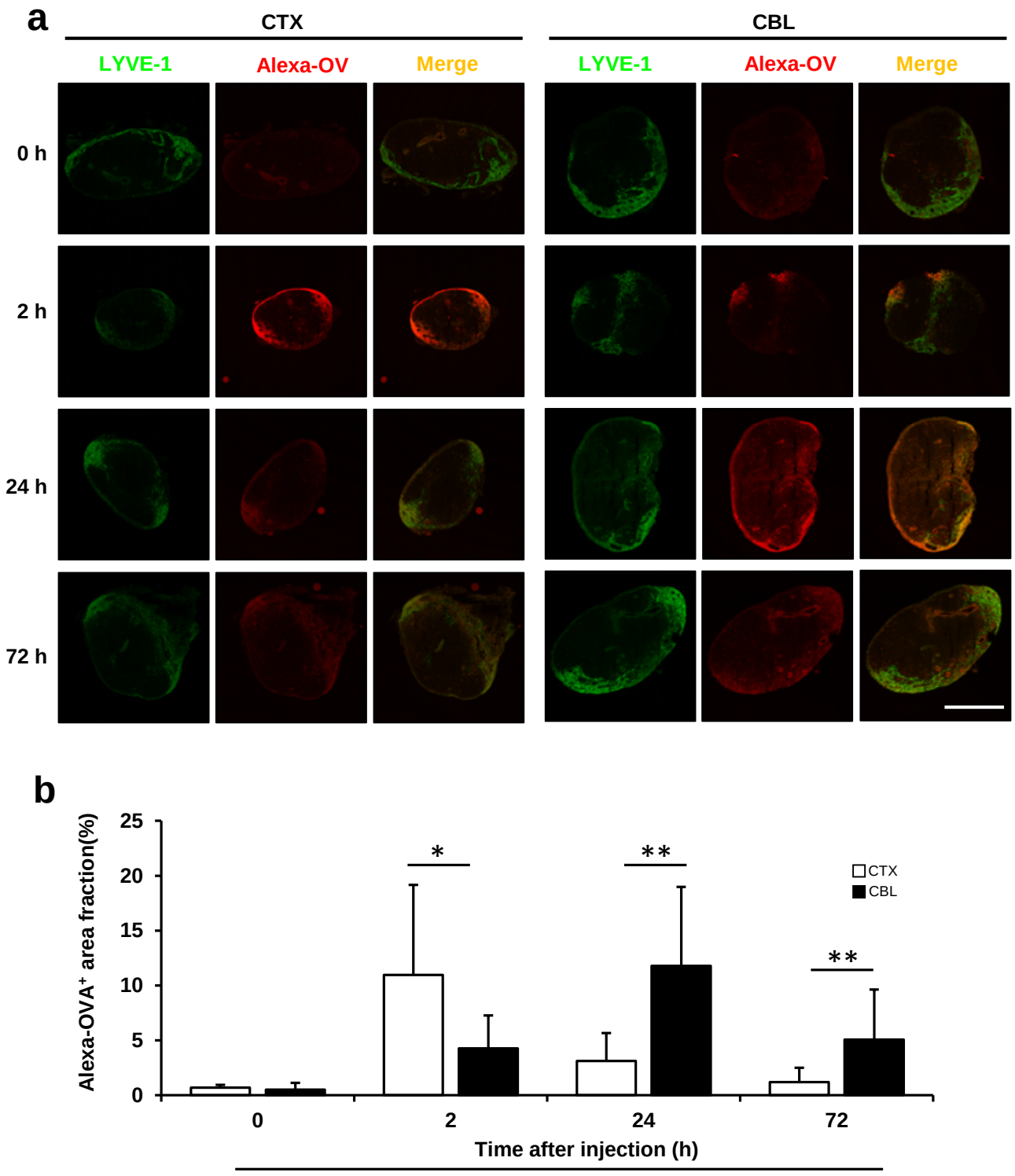

Fig. 20 Drainage of Alexa-OV from brain tissues into DcLNs. (**a**) Detection of brain-injected Alexa-OV in Dclns. Dclns were removed in each tome point after Alexa-OV injection in CTX (left panel) and CBL (right panel). We detected robust Alexa-OV signals in DcLNs in 2 hours after CTX injection and 24 hours after CBL injection. Alexa-OV(red), LYVE-1 (green), and Merge (yellow). Scale bar indicates 500 μm. (**b**) Quantification for Alexa-OV positive area fraction in DcLns sections. Alexa-OV positive area fraction in DcLNs of CTX injection reached at the maximum level at 2 hours while that of CBL maximum at 24 hours and decreased over time respectively. Data represent mean ± SD. n = 3~5 mice per group. *, $p < 0.05$. **, $p < 0.01$ (unpaired *t*-test).

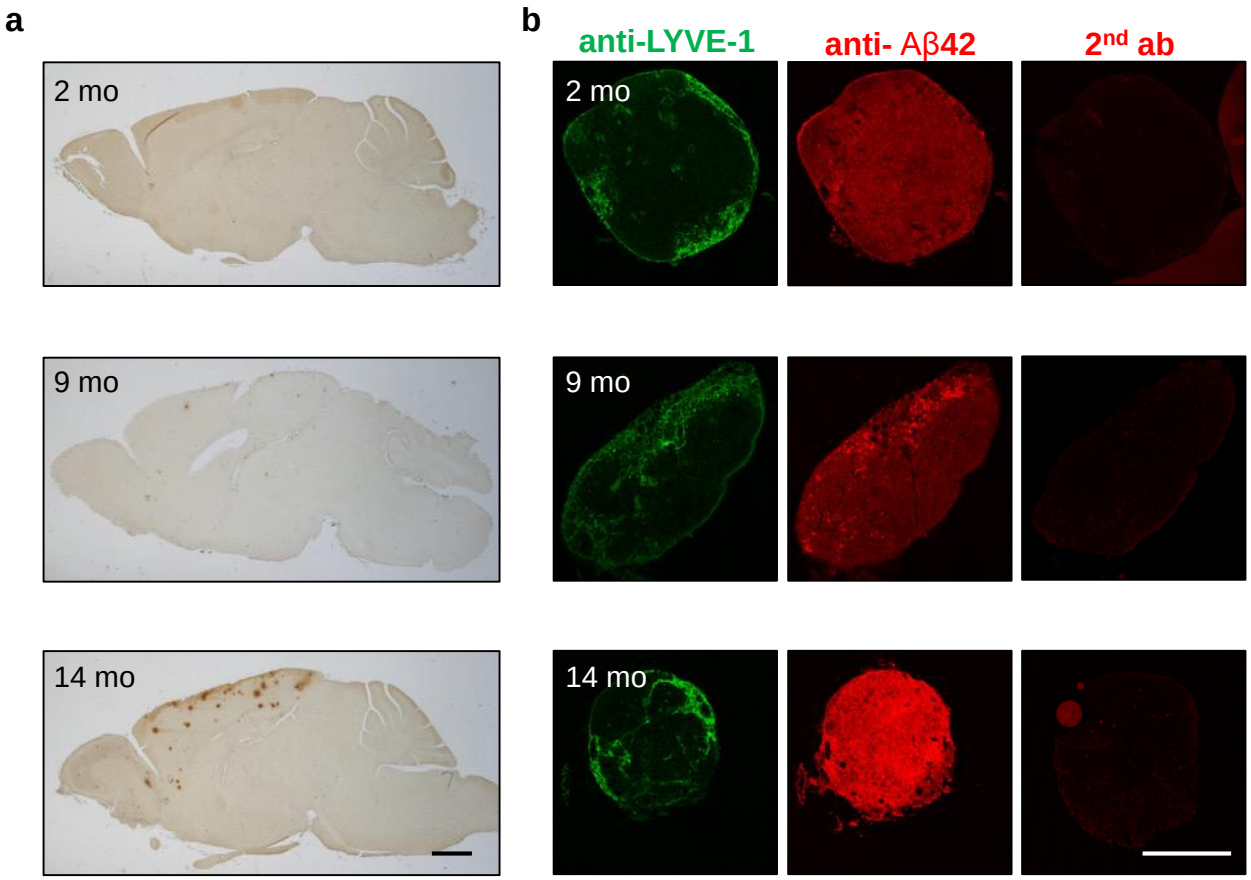

Fig. 21 Detection of endogenous Aβ42 in DcLNs. (**a**) Immunostaining of *APP*$^{NL-F}$ mouse brain sections with anti-Aβ antibody (82E1). Age-dependent Aβ deposition was observed in CTX. No Aβ deposition in CBL was detected even in 14-month old mice. Scale bar indicates 1 mm. (**b**) Dclns were collected and analyzed by immunohistochemistry with anti-lymphatic vessel endothelial hyaluronan receptor-1 (LYVE-1) antibody and anti-Aβ42 antibody in DcLNs. We detected anti-Aβ42 antibody-dependent signals in DcLNs. Treatment of DcLNs specimens with only secondary antibody showed no signal. Scale bar indicates 500 μm. (Shahnur A et al., 2021) [20].

Acknowledgement

First of all, I would like to express my deepest sense of gratitude to my supervisor, Dr. Satoru Funamoto, Laboratory of Neuropathology, Graduate School of Life and Medical Sciences, Doshisha University, for his constant inspiration, scholastic guidance, immense encouragement, valuable suggestion, timely and solitary instruction, cordial behaviors, constructive criticism and providing all facilities for successful completion of the research work.

I would like to convey my eternal gratitude to Dr. Tomohiro Miyasaka and Dr. Nobuto Kakuda, Laboratory of Neuropathology, Graduate School of Life and Medical Sciences, Doshisha University, for their constructive advice, experimental support and active help.

My sincere thanks to Dr. Moniruzzaman Mohammad for sharing experience and knowledge during the time of study as well as all other members of Laboratory of Neuropathology for their kind cooperation in every step of my research.

During of my PhD, first time I get a taste of my fatherhood with a boy Shah Muhammad Samir. I would like to acknowledge a super lady and she is my wife Shahanaz Parvin. Mrs. Parveen has been extremely supportive of me throughout this entire process and has made countless sacrifices to ensure that I can complete this PhD.